PHYSICAL REVIEW D **80,** 034001 (2009)

Analytical results for $O(\alpha_s)$ radiative corrections to $e^+e^- \to t\bar{t}^{\uparrow}$ up to a given gluon energy cut

S. Groote[1,2] and J. G. Körner[1]

[1]*Institut für Physik, Johannes-Gutenberg-Universität, Staudinger Weg 7, 55099 Mainz, Germany*
[2]*Loodus- ja Technoloogiateaduskond, Füüsika Instituut, Tartu Ülikool, Tähe 4, 51010 Tartu, Estonia*
(Received 19 November 2008; published 3 August 2009)

We determine the $O(\alpha_s)$ radiative corrections to polarized top quark pair production in e^+e^- annihilations with a specified gluon energy cut. We write down fully analytical results for the unpolarized and polarized $O(\alpha_s)$ cross sections $e^+e^- \to \bar{t}t(G)$ and $e^+e^- \to \bar{t}t^{\uparrow}(G)$ including their polar orientation dependence relative to the beam direction. In the soft-gluon limit we recover the usual factorizing form known from the soft-gluon approximation. In the limit when the gluon energy cut takes its maximum value we recover the totally inclusive unpolarized and polarized cross sections calculated previously. We provide some numerical results on the cutoff dependence of the various polarized and unpolarized cross sections and discuss how the exact results numerically differ from the approximate soft-gluon results.

DOI: 10.1103/PhysRevD.80.034001 PACS numbers: 12.38.Bx, 14.65.Ha, 13.38.Dg, 13.66.Bc

I. INTRODUCTION

After the discovery of the heavy top quark at the Tevatron in 1995 there has been much interest in the use of the proposed high energy linear e^+e^- collider as a copious source of top quark pairs. When the proposed linear collider ILC comes into operation it is necessary to have available detailed radiative corrections to the production and the decay of top quark pairs. Concerning production there are a number of unpolarized and single spin polarized structure functions that describe the e^+e^- production process of massive top quark pairs. In the unpolarized case one has the three structure functions H_U (unpolarized transverse), H_L (longitudinal), and H_F (forward-backward) which determine the polar angle orientation of the top pair relative to the beam axis. Partial results on the full $O(\alpha_s)$ radiative corrections to the unpolarized structure functions H_U, H_L, and H_F had been written down in Refs. [1,2] starting with the early work on the $O(\alpha)$ QED radiative corrections to the vector current $(\gamma_V e^+e^-)$ vertex function [3]. Complete results on the $O(\alpha_s)$ unpolarized structure functions have been first given in Refs. [4,5]. All of the unpolarized $O(\alpha_s)$ structure functions were recalculated in the course of computing the top quark's $O(\alpha_s)$ polarization asymmetries where the unpolarized structure functions were needed to normalize the polarization asymmetries [6–10]. The numerators of the polarization asymmetries are expressed in terms of polarized structure functions. In the case of the longitudinal polarization of the top, one has the three structure functions H_U^l, H_L^l, and H_F^l for which the full $O(\alpha_s)$ radiative corrections were given in Refs. [7,8,10]. In the case of a top quark polarized transverse or normal to the event plane, one has two structure functions in each case which are H_I^T and H_A^T, and H_I^N and H_A^N, respectively (see e.g. Ref. [9]). These were calculated in Refs. [9,11].

When doing the full $O(\alpha_s)$ radiative corrections one integrates over the full (hard and soft) gluon phase space. For some applications it is also interesting to consider radiative corrections where one integrates over gluon phase space up to a given gluon energy cut E_c.[1] Such radiative corrections may be dictated by experimental considerations when soft gluons accompanying the top quark pair cannot be resolved by the detector. Alternatively one could attempt to measure the cross section for top-antitop-gluon production with a given gluon energy cut E_c and compare the energy cut dependence of the cross section with the predictions of QCD. Finally, one could define a hard gluon region by introducing a lower gluon energy cut and compare experiment with QCD in the hard gluon region.

In this paper we provide analytical results for the $O(\alpha_s)$ radiative corrections to the three unpolarized structure functions H_U, H_L, and H_F as well as for the seven polarized structure functions H_U^ℓ, H_L^ℓ, H_F^ℓ, $H_I^{T,N}$, and $H_A^{T,N}$ for polarized top quarks where we integrate over the gluon energy phase space up to a given energy cut E_c. We mention that radiative corrections with a gluon energy cut have been treated before in the unpolarized case [12,13].

We emphasize that we are not using the soft-gluon approximation (SGA) in the present calculation but integrate over the full $O(\alpha_s)$ matrix element tree graph structure. However, we will compare our results with the soft-gluon approximation. The soft-gluon approximation consists of the factorization of the tree graph contribution into the Born term contribution and a universal soft-gluon piece which can be easily integrated. An $O(\alpha_s)$ calculation of some of the structure functions appearing in polarized top pair production using variants of the soft-gluon approximation has been done before in Refs. [10,14].

One of the further aims of the present investigation is to find out to what extent one can pin down a new non-SM (standard model) coupling structure in top quark pair pro-

[1]Technically, this means that one is dealing with a three-scale problem with the scales q^2, m_t, and E_c.

duction in the presence of $O(\alpha_s)$ radiative corrections with an exact treatment of gluon emission rather than soft-gluon emission. In the latter approximation the tree graph contribution is Born termlike and thus polarization-type observables would not be affected by the radiative tree graph corrections but only by the non-Born term structure of the one-loop contributions. Deviations from SM predictions for the polarization-type observables could result from a new non-SM coupling structure or from an exact treatment of radiative corrections. As an example we will introduce an anomalous CP-odd axial current and compare the results of our exact next-to-leading order (NLO) calculation with the contributions of the anomalous axial current for some relevant observables and structure functions.

II. UNPOLARIZED AND POLARIZED STRUCTURE FUNCTIONS

In order to acquaint the reader with our notation, we use this section to outline the main structure of the cross-section calculation and to introduce the various unpolarized and polarized structure functions that come into play. To start with, we define a polarized hadron tensor for the three-body process $(\gamma_V, Z) \to q(p_1) + \bar{q}(p_2) + G(p_3)$ according to

$$H_{\mu\nu}(q, p_1, p_2, s) = \sum_{\bar{q},G \text{ spins}} \langle \bar{q}q(s)G|j_\mu|0\rangle\langle 0|j_\nu^\dagger|\bar{q}q(s)G\rangle, \tag{1}$$

where p_1, p_2, and p_3 are the four-momenta of the quark, antiquark, and gluon, respectively, and $q = p_1 + p_2 + p_3$ is the four-momentum of the intermediate gauge boson. The spin vector of the quark is denoted by s. A similar definition holds for the Born case $(\gamma_V, Z) \to q(p_1) + \bar{q}(p_2)$. The hadron tensor defined in Eq. (1) depends on the vector (V: γ_μ) and axial-vector (A: $\gamma_\mu\gamma_5$) composition of the product of currents j_μ and j_ν. It is convenient to introduce the four independent hadron tensor components $H^i_{\mu\nu}$ $(i = 1, 2, 3, 4)$ defined according to

$$\begin{aligned} H^1_{\mu\nu} &= \frac{1}{2}(H^{VV}_{\mu\nu} + H^{AA}_{\mu\nu}), & H^2_{\mu\nu} &= \frac{1}{2}(H^{VV}_{\mu\nu} - H^{AA}_{\mu\nu}), \\ H^3_{\mu\nu} &= \frac{i}{2}(H^{VA}_{\mu\nu} - H^{AV}_{\mu\nu}), & H^4_{\mu\nu} &= \frac{1}{2}(H^{VA}_{\mu\nu} + H^{AV}_{\mu\nu}). \end{aligned} \tag{2}$$

For notational convenience we have omitted all arguments in the hadron tensor components in Eqs. (2). In the following we will use explicit arguments only when they are needed. For example, we include the spin vector argument when we define unpolarized and polarized structure functions $H^i_{\mu\nu}$ and $H^{i,m}_{\mu\nu}$ $(i = 1, 2, 3, 4, m = \ell, T, N)$ according to

$$\begin{aligned} H^i_{\mu\nu} &= H^i_{\mu\nu}(s^m) + H^i_{\mu\nu}(-s^m), \\ H^{i,m}_{\mu\nu} &= H^i_{\mu\nu}(s^m) - H^i_{\mu\nu}(-s^m), \end{aligned} \tag{3}$$

where s^m is the spin vector corresponding to longitudinal $(m = \ell)$, transverse $(m = T)$, and normal $(m = N)$ polarization of the top quark. Our choices of the three orthonormal spin directions $(\vec{e}_T, \vec{e}_N, \vec{e}_\ell)$ are given by

$$\vec{e}_T = \frac{(\vec{p}_{e^-} \times \vec{p}_1) \times \vec{p}_1}{|(\vec{p}_{e^-} \times \vec{p}_1) \times \vec{p}_1|}, \qquad \vec{e}_N = \frac{\vec{p}_{e^-} \times \vec{p}_1}{|\vec{p}_{e^-} \times \vec{p}_1|}, \qquad \vec{e}_\ell = \frac{\vec{p}_1}{|\vec{p}_1|} \tag{4}$$

(cf. Figure 1). For the hadron tensor components we introduce the compact notation $H^{i(m)}_{\mu\nu}$ where the round brackets indicate that, in the unpolarized case, the index m and the round bracket is omitted. We use this compact notation to display the general features common to the unpolarized and polarized parts.

For the process $e^+e^- \to \bar{q}q(G)$, the cross section can be written in modular form consisting of the hadron tensor, the lepton tensor, and the model dependent coupling coefficients g_{ij}. The SM values of the coupling coefficients g_{ij} are listed in Appendix A. The unpolarized and polarized cross sections read

$$d\sigma^{(m)} = \frac{e^4}{2q^6} \sum_{i,j=1}^{4} g_{ij} L^{i\mu\nu} H^{j(m)}_{\mu\nu} dPS, \tag{5}$$

where dPS is the phase-space factor. The lepton tensor components $L^i_{\mu\nu}$ $(i = 1, 2, 3, 4)$ are defined in the same way as in Eq. (2). The process $e^+e^- \to \bar{q}q(G)$ can be described either in the *beam* plane spanned by the electron and positron beam and the outgoing quark, or the *event* plane spanned by the quark, the antiquark, and the gluon. In the Born case where no gluon is emitted, both planes coincide by convention. The polar angle between the quark momentum and the electron momentum is denoted by θ (or by θ_{te^-}), and the azimuthal angle between the two planes is denoted by χ. In order to determine directions, we define different frames with the (x, z) plane lying in the corresponding plane. For the beam plane we define a *lepton*

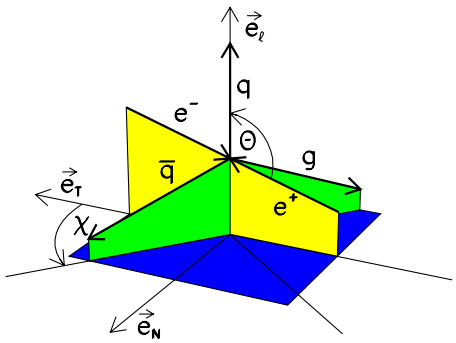

FIG. 1 (color online). Orthonormal spin basis $\vec{e}_T$, $\vec{e}_N$, and $\vec{e}_\ell$ for the top quark. Also shown are the beam plane (light gray, respectively, yellow) and the event plane (dark gray, respectively, green).

frame with the z axis determined by the momentum direction of the electron, and a *beam* frame with the z axis determined by the momentum direction of the quark. For the event plane we define an *event* frame with the z direction determined again by the momentum direction of the quark. The transition from one frame to the other is performed by using the two Euler angles θ and χ.

The natural frame for describing the hadron tensor is the event frame which makes no reference to the beam plane. On the other hand, the lepton tensor is most naturally described in the lepton frame. In this frame the lepton tensor component $L^{3\mu\nu}$ vanishes identically and $L^{2\mu\nu}$ vanishes for zero lepton masses (which we assume). The remaining two components have the simple form

$$L^{1\mu\nu} = \frac{q^2}{2}\begin{pmatrix} 0 & 0 & 0 & 0 \\ 0 & 1 & 0 & 0 \\ 0 & 0 & 1 & 0 \\ 0 & 0 & 0 & 0 \end{pmatrix},$$
$$L^{4\mu\nu} = \frac{q^2}{2}\begin{pmatrix} 0 & 0 & 0 & 0 \\ 0 & 0 & -i & 0 \\ 0 & i & 0 & 0 \\ 0 & 0 & 0 & 0 \end{pmatrix}. \tag{6}$$

The contraction of the lepton and hadron tensor has to be done in one particular frame for which we choose the event frame. We therefore have to rotate the lepton tensor into the event frame. In doing so a variety of angular dependences appear. In fact we can decompose the lepton tensors according to

$$L^{1\mu\nu} = \frac{q^2}{2}\left\{\frac{1}{2}(1+\cos^2\theta)\Pi_U^{\mu\nu} + \sin^2\theta\Pi_L^{\mu\nu} - 2\sqrt{2}\sin\theta\cos\theta\Pi_I^{\mu\nu}\right\},$$
$$L^{4\mu\nu} = \frac{q^2}{2}\left\{\cos\theta\Pi_F^{\mu\nu} - 2\sqrt{2}\sin\theta\Pi_A^{\mu\nu}\right\}, \tag{7}$$

where Π_I and Π_A contain an implicit linear dependence on $\sin\chi$ and $\cos\chi$. The matrices $\Pi_U, \Pi_L, \Pi_I, \Pi_F$, and Π_A are called *projectors* because when contracting the lepton tensor with the hadron tensor they project out the relevant coefficients of the hadron tensor that give rise to the various angular dependences. The decomposition in Eq. (7) describes the complete angular dependence of unpolarized and polarized top production in the process $e^+e^- \to \bar{q}q(G)$. It gives rise to the decomposition of the differential cross section according to

$$\frac{d\sigma^{(m)}}{d\cos\theta} = \frac{3}{8}(1+\cos^2\theta)\sigma_U^{(m)} + \frac{3}{4}\sin^2\theta\sigma_L^{(m)} + \frac{3}{4}\cos\theta\sigma_F^{(m)} - \frac{3}{\sqrt{2}}\sin\theta\cos\theta\sigma_I^{(m)} - \frac{3}{\sqrt{2}}\sin\theta\sigma_A^{(m)}, \tag{8}$$

where

$$\sigma_a^{(m)} = \frac{(4\pi\alpha)^2}{3q^4}\sum_{j=1}^{4} g_{ij}\int H_a^{j(m)}\frac{dPS}{d\cos\theta},$$
$$H_a^{j(m)} = \Pi_a^{\mu\nu}H_{\mu\nu}^{j(m)}. \tag{9}$$

Without beam polarization effects one finds the following pattern. For $i=1$ one has contributions from $a = U, L, I$ and for $i=4$ one has contributions from $a = F, A$ as written out in Eq. (7). More details about the coupling pattern including transverse and longitudinal beam polarization effects can be found in [10]. In Eqs. (9) we have divided out the $d\cos\theta$ differential which has already been taken into account in the polar distribution (8). For the two-particle final states (Born term and loop contribution) one has the phase-space factor

$$dPS_2 = \frac{v}{8(2\pi)^2}d\cos\theta d\chi \to \frac{v}{16\pi}d\cos\theta, \tag{10}$$

where $v = \sqrt{1-4m^2/q^2}$ is the velocity of the outgoing quark. The transition to the rightmost form in Eq. (10) marked by an arrow expresses the fact that the azimuthal integration over χ is always implied throughout this paper. As we shall see, the transverse and normal spin dependence drop out for the components $a = U, L, F$ in $H_a^{j(m)}$ but are retained for the components $a = I, A$ after the azimuthal integration over χ.[2] Just the opposite happens to the spin independent and longitudinal spin components. For the two-particle final state one obtains

$$\sigma_a^{(m)}(\text{Born, loop}) = \frac{\pi\alpha^2 v}{3q^4}\sum_{j=1}^{4} g_{ij}H_a^{j(m)}(\text{Born, loop}) \tag{11}$$

with $a = U, L, I$ for $i=1$ and $a = F, A$ for $i=4$ as above.

Next we turn to the $O(\alpha_s)$ tree graph contributions. The relevant three particle final state phase space is given by

$$dPS_3 = \frac{v}{8(2\pi)^2}d\cos\theta d\chi\frac{q^2}{16\pi^2 v}dydz \to \frac{v}{16\pi}d\cos\theta\frac{q^2}{16\pi^2 v}dydz, \tag{12}$$

where the transition to the last expression is again due to the azimuthal integration. We have introduced two phase-space variables $y = 1 - 2p_1\cdot q/q^2$ and $z = 1 - 2p_2\cdot q/q^2$. The $O(\alpha_s)$ tree graph contributions to the various cross sections $\sigma_a^{(m)}$ are written as

[2]It is important to keep in mind that the transverse and normal spin components are defined with respect to the beam frame. When defined with respect to the event frame the transverse and normal spin components average to zero after azimuthal averaging.

$$\sigma_a^{(m)}(\text{tree}) = \frac{\pi\alpha^2 v}{3q^4}\left(\frac{q^2}{16\pi^2 v}\sum_{j=1}^{4} g_{ij}\int H_a^{j(m)}(y,z)dydz\right) \tag{13}$$

with $a = U, L, I$ for $i = 1$ and $a = F, A$ for $i = 4$, as before. It is convenient to introduce the tree graph helicity structure functions $H_a^{j(m)}(\text{tree})$ by defining

$$H_a^{j(m)}(\text{tree}) = \frac{q^2}{16\pi^2 v}\int H_a^{j(m)}(y,z)dydz. \tag{14}$$

The Born term and the $O(\alpha_s)$ corrections $H_a^{j(m)}(\text{Born})$ and $H_a^{j(m)}(\alpha_s) = H_a^{j(m)}(\text{tree}) + H_a^{j(m)}(\text{loop})$ will be referred to as the *unpolarized* and *polarized* structure functions to leading (LO) and NLO order, respectively, while the sum of the LO and NLO contributions will be referred to as the $O(\alpha_s)$ results.

In summary, one has three unpolarized and seven polarized hadronic helicity structure functions. It is instructive to list them together including a specification of whether they are fed by the parity conserving (pc) or by the parity violating $(p\upsilon)$ part of the product of hadronic currents and to which of the two classes of the so-called T-even and T-odd structure functions they belong to. One has

$$\text{unpolarized}: H_U(pc), H_L(pc), H_F(p\upsilon) \qquad T\text{-even}, \tag{15}$$

$$\text{longitudinally polarized}: H_U^\ell(p\upsilon), H_L^\ell(p\upsilon), H_F^\ell(pc) \quad T\text{-even}, \tag{16}$$

$$\text{transversely polarized}: H_A^T(pc), H_I^T(p\upsilon) \qquad T\text{-even}, \tag{17}$$

$$\text{normal polarization}: H_I^N(pc), H_A^N(p\upsilon) \qquad T\text{-odd}. \tag{18}$$

If one neglects contributions proportional to the imaginary part $\text{Im}\chi_Z$ of the Breit-Wigner line shape of the Z boson (see Appendix A) the T-odd helicity structure functions $H_A^N(p\upsilon)$ and $H_I^N(pc)$ are contributed to by the imaginary parts of the one-loop amplitudes leading to nonvanishing triple product correlations of the type $\vec{s}_t \cdot (\vec{l} \times \vec{p}_t)$, whereas the T-even structure functions obtain contributions from the Born term, the $O(\alpha_s)$ tree graph contributions, and the real part of the one-loop contributions.

If one includes the contributions proportional to the imaginary part $\text{Im}\chi_Z$ the structure functions $H_F(p\upsilon)$, $H_U^\ell(p\upsilon)$, and $H_I^T(p\upsilon)$ are also contributed to by the imaginary parts of the one-loop contributions, and, vice versa, $H_A^N(p\upsilon)$ obtains also contributions from the Born term, the $O(\alpha_s)$ tree graph contributions, and the real part of the one-loop contributions. All the latter contributions originate from the $(VA - AV)$ part of the product of hadron currents and thus belong to the class of helicity structure functions $H_a^{3(m)}$ according to the classification of Eq. (2). The latter contributions can only be probed through the imaginary part of the Breit-Wigner resonance shape which is strongly suppressed for $(t\bar{t})$ production. In fact, the contributions coming from the imaginary part of the Breit-Wigner resonance shape are of order $O(\text{Im}\chi_Z(q^2)/\text{Re}\chi_Z(q^2))$ and can thus safely be neglected for top quark pair production. For example, in the threshold region of top quark pair production $\text{Im}\chi_Z/\text{Re}\chi_Z$ is approximately 0.1% and decreases further with a $1/q^2$ power falloff behavior. We shall nevertheless include all $H_a^{3(m)}$ contributions for completeness and for possible applications in $(b\bar{b})$ production where the $H_a^{3(m)}$ contributions cannot be neglected in the Z resonance region.

III. COVARIANT EXPRESSIONS FOR THE PROJECTORS

The projectors Π_a will be written in covariant form. We go to the rest frame of the gauge boson such that $q = (\sqrt{q^2}; 0, 0, 0)$. The z axis is defined by the momentum direction of the top quark. For the top quark momentum one has

$$p_1 = \frac{1}{2}\sqrt{q^2}(1 - y; 0, 0, \sqrt{(1-y)^2 - \xi}) \tag{19}$$

$(y = 0$ for two-body decays) with $\xi = 1 - v^2 = 4m^2/q^2$. We construct a four-transverse quark momentum and a four-transverse metric tensor

$$\begin{aligned} \hat{g}_{\mu\nu} &= g_{\mu\nu} - \frac{q_\mu q_\nu}{q^2}, \\ \hat{p}_{1\mu} &= \hat{g}_{\mu\nu}p_1^\nu = p_{1\mu} - \frac{p_1 \cdot q}{q^2}q_\mu \end{aligned} \tag{20}$$

and use q and $\hat{p}_1$ to build up two elements of a coordinate basis,

$$e_0^\mu = (q^\mu/\sqrt{q^2}) \times (= (1; 0, 0, 0) \text{ in the gauge boson rest system}), \tag{21}$$

$$e_3^\mu = (\hat{p}_1^\mu/\sqrt{(p_1 \cdot q)^2/q^2 - m^2}) \times (= (0; 0, 0, 1) \text{ in the gauge boson rest system}). \tag{22}$$

In covariant form the longitudinal spin vector of the top quark reads (see e.g. [15])

$$s^{\ell\mu} = -\left(q^\mu - \frac{p_1 q}{m^2}p_1^\mu\right)\Big/\sqrt{(p_1 q)^2/m^2 - q^2}. \tag{23}$$

In the gauge boson rest system Eq. (23) turns into

$$s^\ell = \frac{1}{\sqrt{\xi}}(\sqrt{(1-y)^2-\xi}; 0, 0, 1-y), \tag{24}$$

while in the top quark rest system one has $s^\ell = (0; 0, 0, 1)$. The longitudinal spin vector s^ℓ can be seen to be a linear combination of the two basis vectors e_0 and e_3 and does not provide a new direction in our vierbein basis. The projectors that can be constructed with the help of e_0 and e_3 are limited to the three projectors

$$\begin{aligned} \Pi_U^{\mu\nu} &= -\hat{g}^{\mu\nu} - e_3^\mu e_3^\nu, \qquad \Pi_L^{\mu\nu} = e_3^\mu e_3^\nu, \\ \Pi_F^{\mu\nu} &= i\varepsilon_{\mu\nu\rho\sigma} e_3^\rho e_0^\sigma, \end{aligned} \tag{25}$$

where $\varepsilon_{\mu\nu\rho\sigma}$ is the totally antisymmetric Levi-Cività tensor with $\varepsilon_{0123} = 1$. They project out the three unpolarized and three longitudinally polarized helicity structure functions where, according to Eq. (3), the polarized structure functions $H_a^{i\ell}$ $(a = U, L, F)$ are obtained from $H_a^{i\ell} = \Pi_a^{\mu\nu}(H_{\mu\nu}^i(s^\ell) - H_{\mu\nu}^i(-s^\ell))$.

The transverse and normal polarization vectors of the top quark are defined in the beam frame. Viewed from the event frame they are given by

$$e_T = (0; \cos\chi, -\sin\chi, 0), \qquad e_N = (0; \sin\chi, \cos\chi, 0). \tag{26}$$

These two vectors therefore allow one to span the beam plane and a plane perpendicular to the beam plane in event frame coordinates. With these new elements it is possible to construct the remaining additional projectors. They read $(m = T, N)$

$$\begin{aligned} \Pi_I^{\mu\nu}(e_m) &= \frac{-1}{2\sqrt{2}}(s^\mu e_3^\nu + e_3^\mu e_m^\nu), \\ \Pi_I'^{\mu\nu}(e_m) &= \frac{-1}{2\sqrt{2}}(\varepsilon_{\mu\rho\sigma\tau} e_3^\nu + \varepsilon_{\nu\rho\sigma\tau} e_3^\mu) e_0^\rho e_3^\sigma e_m^\tau, \\ \Pi_A^{\mu\nu}(e_m) &= \frac{-i}{2\sqrt{2}}\varepsilon_{\mu\nu\rho\sigma} e_0^\rho e_m^\sigma, \\ \Pi_A'^{\mu\nu}(e_m) &= \frac{i}{2\sqrt{2}}(e_m^\mu e_3^\nu - e_3^\mu e_m^\nu). \end{aligned} \tag{27}$$

For example, according to Eq. (3), one obtains the structure function H_I^{4T} by calculating $H_I^{4T} = \Pi_I^{\mu\nu}(e_T) \times (H_{\mu\nu}^4(s^T) - H_{\mu\nu}^i(-s^T))$. Note that since $\Pi_I(e_N) = \Pi_I'(e_T)$, $\Pi_I(e_T) = -\Pi_I'(e_N)$, $\Pi_A(e_N) = -\Pi_A'(e_T)$, and $\Pi_A(e_T) = \Pi_A'(e_N)$, the primed projectors are redundant. This set of four [Eq. (27)] and six [Eq. (25)] covariant projectors allows one to calculate the complete set of ten helicity structure functions from the hadron tensor.

In the following we list the Born term and loop contributions calculated already in previous papers [8–10]. The nonvanishing unpolarized Born term contributions are given by

$$\begin{aligned} H_U^1(\text{Born}) &= 2N_c q^2(1+v^2), \\ H_L^1(\text{Born}) &= N_c q^2(1-v^2) = H_L^2(\text{Born}), \\ H_U^2(\text{Born}) &= 2N_c q^2(1-v^2), \\ H_F^4(\text{Born}) &= 4N_c q^2 v. \end{aligned} \tag{28}$$

The longitudinally polarized contributions read

$$\begin{aligned} H_U^{4\ell}(\text{Born}) &= 4N_c q^2 v, \qquad H_F^{1\ell}(\text{Born}) = 2N_c q^2(1+v^2), \\ H_L^{4\ell}(\text{Born}) &= 0, \qquad H_F^{2\ell}(\text{Born}) = 2N_c q^2(1-v^2). \end{aligned} \tag{29}$$

For the transverse and normal polarization components one has [9]

$$\begin{aligned} H_I^{4T}(\text{Born}) &= N_c q^2 v\sqrt{\frac{\xi}{2}}, \\ H_A^{1T}(\text{Born}) &= N_c q^2\sqrt{\frac{\xi}{2}} = H_A^{2T}(\text{Born}), \\ H_A^{3N}(\text{Born}) &= N_c q^2 v\sqrt{\frac{\xi}{2}}. \end{aligned} \tag{30}$$

Note that one has $H_L^1 = H_L^2, H_U^1 = H_F^{1\ell}, H_U^2 = H_F^{2\ell}, H_F^4 = H_U^{4\ell}, H_A^{1T} = H_A^{2T}$, and $H_I^{4T} = H_A^{3N}$ at the Born term level. We will return to these relations when we discuss the $O(\alpha_s)$ tree graph contributions.

Note that the transverse and normal spin components T and N are proportional to $\sqrt{\xi} = 2m/\sqrt{q^2}$. The origin of this suppression factor is a helicity flip suppression factor at the $\gamma/Z - t\bar{t}$ vertex. The same suppression factor also occurs in the $O(\alpha_s)$ one-loop and tree graph radiative corrections to be treated later on. It is clear that this overall suppression factor is not important for $(t\bar{t})$ production in the threshold region and not very significant in the range of beam energies considered in this paper. Altogether this means that the transverse and normal spin components of the top quark are non-negligible in the present application [9,11].

Most of the nonvanishing one-loop contributions have already been given in [8–10]

$$
\begin{aligned}
&H_U^1(\text{loop}) = 4N_c q^2((1+v^2)\,\text{Re}A - 2v^2\,\text{Re}B), \qquad H_U^2(\text{loop}) = 4N_c q^2((1-v^2)\,\text{Re}A + 2v^2\,\text{Re}B),\\
&H_L^1(\text{loop}) = 2N_c q^2((1-v^2)\,\text{Re}A + v^2\,\text{Re}B) = H_L^2(\text{loop}), \qquad H_F^3(\text{loop}) = -8N_c q^2 v\,\text{Im}B,\\
&H_F^4(\text{loop}) = 8N_c q^2 v(\text{Re}A - \text{Re}B), \qquad H_U^{3\ell}(\text{loop}) = -8N_c q^2 v\,\text{Im}B, \qquad H_U^{4\ell}(\text{loop}) = 8N_c q^2 v(\text{Re}A - \text{Re}B),\\
&H_L^{3\ell}(\text{loop}) = 0 = H_L^{4\ell}(\text{loop}), \qquad H_F^{1\ell}(\text{loop}) = 4N_c q^2((1+v^2)\,\text{Re}A - 2v^2\,\text{Re}B),\\
&H_F^{2\ell}(\text{loop}) = 4N_c q^2((1-v^2)\,\text{Re}A + 2v^2\,\text{Re}B), \qquad H_I^{3T}(\text{loop}) = -N_c q^2 v\sqrt{\frac{\xi}{2}}(1+\xi)\,\text{Im}B/\xi,\\
&H_I^{4T}(\text{loop}) = N_c q^2 v\sqrt{\frac{\xi}{2}}(2\,\text{Re}A + (1-3\xi)\,\text{Re}B/\xi), \qquad H_A^{1T}(\text{loop}) = N_c q^2\sqrt{\frac{\xi}{2}}(\text{Re}A + v^2\,\text{Re}B/\xi) = H_A^{2T}(\text{loop}),\\
&H_I^{1N}(\text{loop}) = N_c q^2\sqrt{\frac{\xi}{2}}(1-\xi)\,\text{Im}B/\xi = H_I^{2N}(\text{loop}),\\
&H_A^{3N}(\text{loop}) = N_c q^2 v\sqrt{\frac{\xi}{2}}(2\,\text{Re}A + (1-3\xi)\,\text{Re}B/\xi), H_A^{4N}(\text{loop}) = N_c q^2 v\sqrt{\frac{\xi}{2}}(1+\xi)\,\text{Im}B/\xi,
\end{aligned}
\tag{31}
$$

where the real part of the form factor A and the real and imaginary parts of the form factor B read

$$
\begin{aligned}
\text{Re}A &= -\frac{\alpha_s C_F}{4\pi}\left\{\left(2 + \frac{1+v^2}{v}\ln\left(\frac{1-v}{1+v}\right)\right)\ln\left(\frac{\Lambda q^2}{m^2}\right) + 3v\ln\left(\frac{1-v}{1+v}\right) + 4 + \frac{1+v^2}{v}\left(\text{Li}_2\left(\frac{2v}{1+v}\right) + \frac{1}{4}\ln^2\left(\frac{1-v}{1+v}\right) - \frac{\pi^2}{2}\right)\right\},\\
\text{Re}B &= \frac{\alpha_s C_F}{4\pi}\frac{1-v^2}{v}\ln\left(\frac{1-v}{1+v}\right), \qquad \text{Im}B = \frac{\alpha_s C_F}{4\pi}\frac{1-v^2}{v}\pi.
\end{aligned}
\tag{32}
$$

The imaginary contributions $H_F^3(\text{loop})$ and $H_U^{3\ell}(\text{loop})$ complete the list of one-loop contributions given in [8–10]. We are now in full agreement with the one-loop contributions given in [11]. ImB contributes to the T-odd structure functions H_I^{4T} and H_A^{4N} as mentioned after Eq. (18). The infrared singularity has been regularized by the introduction of a gluon mass m_G via $m_G^2 = \Lambda q^2$. The loop induced infrared singularities in the real part of the one-loop contributions can be seen to cancel against the corresponding infrared singularities in the tree graph contributions to be treated later on.

In the next section we will present our results on the cutoff dependent helicity structure functions. They must coincide with the fully integrated results written down in Refs. [8–10] when the cutoff is taken to its maximal value $E_G(\text{max}) = (q^2 - 4m^2)/(2\sqrt{q^2})$. This will be verified in Sec. V.

IV. EXACT RESULT UP TO A GIVEN GLUON ENERGY CUT

In this section we present the results of our calculations for the $O(\alpha_s)$ corrections to the helicity structure functions with a given cut on the gluon energy. We define a scaled gluon energy cut $\lambda = E_G/\sqrt{q^2}$ and do the phase-space integration in the region $0 \le E_G \le \lambda_{\text{max}}\sqrt{q^2}$. The maximal value that the cut parameter λ can take is $\lambda_{\text{max}} = (1 - \xi)/2$. In terms of our phase-space variables y and z the cut phase space is defined by $0 \le y + z \le 2\lambda$. In Fig. 2 we have drawn a (y, z) phase-space plot choosing a specific value for $\xi = 0.1$ for illustrative purposes. The shaded area

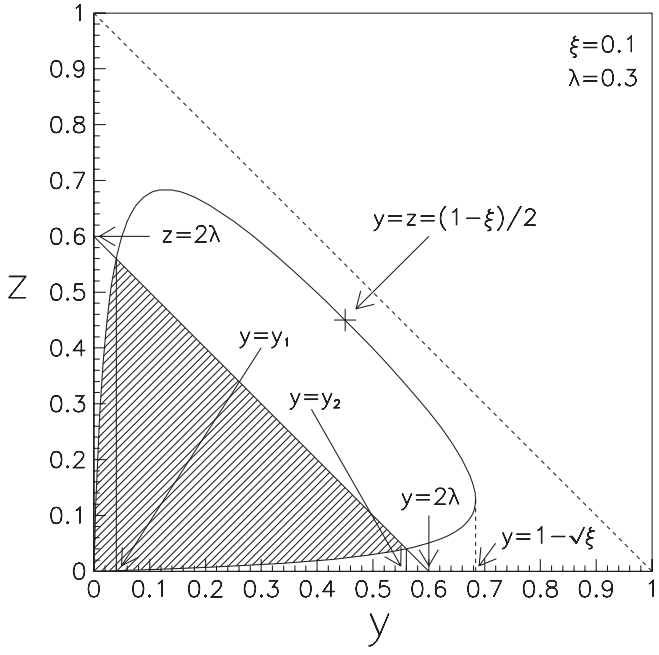

FIG. 2. Phase-space diagram with gluon cut.

corresponds to the integration region with the specific choice of cut value $\lambda = 0.3$. The upper boundary of the integration region is given by the straight line $z = -y + 2\lambda$.

The full phase space is bounded from above and below by the two functions z_+ and z_- where

$$z_\pm = \frac{2y - 2y^2 - \xi y \pm 2y\sqrt{(1-y)^2 - \xi}}{4y + \xi}. \tag{33}$$

The upper gluon cut given by $z = -y + 2\lambda$ intersects the two boundary curves (33) at

$$\begin{aligned} y_1 &= \lambda\left(1 - \sqrt{\frac{1 - 2\lambda - \xi}{1 - 2\lambda}}\right), \\ y_2 &= \lambda\left(1 + \sqrt{\frac{1 - 2\lambda - \xi}{1 - 2\lambda}}\right). \end{aligned} \tag{34}$$

Since the phase space is symmetric with respect to reflections along the diagonal, the corresponding z values are $z_1 = y_2$ and $z_2 = y_1$.

From a visual inspection of the phase-space plot, Fig. 2, one can see that one has to discuss two cases when integrating the cut phase space depending on whether (case A) $\lambda \le \lambda_{\text{trans}}$ or (case B) $\lambda > \lambda_{\text{trans}}$. The transition value $\lambda_{\text{trans}} = (1 - \sqrt{\xi})/(2 - \sqrt{\xi})$ is defined by the λ value at which the straight boundary line of the cut intersects the phase-space boundary at the point $(y_2, z_2) = (1 - \sqrt{\xi}, \sqrt{\xi}(1 - \sqrt{\xi})/(2 - \sqrt{\xi}))$. At this point the tangent of the full phase-space boundary is vertical. From an inspection of the phase-space plot, Fig. 2, one concludes that in case A the integration region is divided into two parts, whereas one has to consider three integration regions in case B. The specific example shown in Fig. 2 corresponds to case A.

Let us denote the general y- and z-dependent tree graph integrands in case A by $I(y, z)$. One has to do the two integrations

$$\int_0^{y_1} \int_{z_-}^{z_+} I(y,z)dydz + \int_{y_1}^{y_2} \int_{z_-}^{2\lambda - y} I(y,z)dydz, \tag{35}$$

while in case B one has an additional integration, viz.

$$\begin{aligned} &\int_0^{y_1} \int_{z_-}^{z_+} I(y,z)dydz + \int_{y_1}^{y_2} \int_{z_-}^{2\lambda - y} I(y,z)dydz \\ &+ \int_{y_2}^{1-\sqrt{\xi}} \int_{z_-}^{z_+} I(y,z)dydz. \end{aligned} \tag{36}$$

It is clear that one should recover the fully integrated results listed in Sec. V when setting λ to its maximal value $\lambda_{\max} = (1 - \xi)/2$. When comparing to the fully integrated result one has to discuss case B with $\lambda = \lambda_{\max} = y_1 = y_2 = (1 - \xi)/2$. In this case the second integral in Eq. (36) vanishes and the remaining two integrals can be merged to give

$$\int_0^{1-\sqrt{\xi}} \int_{z_-}^{z_+} I(y,z)dydz \tag{37}$$

which corresponds to the fully integrated tree graph contribution entering the full NLO result given in Sec. V.

Let us return to case A involving the two integrations in Eq. (35). For most practical applications case A will be the relevant case since the ratio

$$\frac{\lambda_{\text{trans}}}{\lambda_{\max}} = \frac{2}{(1 + \sqrt{\xi})(2 - \sqrt{\xi})} \tag{38}$$

remains close to 1 over most of the range of ξ values. The integration over z is straightforward. The second integration over y is done by using the Euler substitution

$$y = 1 - \sqrt{\xi}\frac{1 + w^2}{1 - w^2}. \tag{39}$$

Equation (39) is easily inverted. The y-integration limits $y = 0$, y_1, y_2, 2λ, and $1 - \sqrt{\xi}$ translate into $w = w_0$, w_1, w_2, w_λ, and 0, where

$$\begin{aligned} w_0 &= \sqrt{\frac{1 - \sqrt{\xi}}{1 + \sqrt{\xi}}} \qquad w_{1,2} = \sqrt{\frac{1 - y_{1,2} - \sqrt{\xi}}{1 - y_{1,2} + \sqrt{\xi}}}, \\ w_\lambda &= \sqrt{\frac{1 - 2\lambda - \sqrt{\xi}}{1 - 2\lambda + \sqrt{\xi}}}. \end{aligned} \tag{40}$$

The value w_λ corresponds to the intersection of the upper gluon cut boundary with any of the two axes. In addition to the velocity parameter $v = \sqrt{1 - \xi}$ we introduce modified velocity parameters $v_i = \sqrt{(1 - y_i)^2 - \xi}$ and $v_\lambda = \sqrt{(1 - 2\lambda)^2 - \xi}$. We shall also use the abbreviations $a = 2 + \sqrt{\xi}$ and $b = 2 - \sqrt{\xi}$. Our results for case A read ($N = \alpha_s N_c C_F q^2/(4\pi v)$)

$$
\begin{aligned}
H_U^1 = N\Big\{&2(2-\xi)^2(t_{0-}-t_{0+}) - (8-10\xi-\xi^2)(t_{1-}-t_{1+}) + \sqrt{\xi}(1-\sqrt{\xi})(2+4\sqrt{\xi}-3\xi)t_w - (6-11\xi)v \\
&+ 2(2-\xi)\ell_{4+} - 16\xi\ell_{5+} - \frac{1}{4}(8+12\xi-\xi^2)\ell_{6+} + \left(16\lambda - 8\lambda^2 - 2\xi + \xi^2 - \frac{4\lambda^2\xi^2}{v_\lambda^2}\right)\ell_{7+} \\
&- \left(16\lambda - 6\lambda^2 - 2(1+4\lambda+\lambda^2)\xi + \xi^2 - \frac{2\lambda^2}{v^2}\right)\ell_{8+} + 2y_1(4-y_1)\ell_1 - 2y_2(4-y_2)\ell_2 - \frac{2(1-2\lambda-(1-\lambda)\sqrt{\xi})}{(1-\sqrt{\xi})\sqrt{\xi}} \\
&\times \left((1-2\lambda)(2-\xi) + 2\lambda\sqrt{\xi} - (4+3\lambda)\xi\sqrt{\xi} + 3\xi^2 - \frac{4\lambda^2\xi\sqrt{\xi}}{1-2\lambda-\sqrt{\xi}}\right)\ell_3 - \frac{1}{4}(24+5\xi)v_1 + \frac{b\xi\sqrt{\xi}}{2(b-aw_1)} \\
&- \frac{1}{4}(48+5\xi)y_1 + 6y_1^2 - \frac{1}{4}(24+5\xi)v_2 - \frac{b\xi\sqrt{\xi}}{2(b+aw_2)} + \frac{1}{4}(48+5\xi)y_2 - 6y_2^2\Big\}, \\
H_U^2 = \xi N\Big\{&2(2-\xi)(t_{0-}-t_{0+}) - (4-\xi)(t_{1-}-t_{1+}) + \sqrt{\xi}(1-\sqrt{\xi})t_w + 2v + 2\ell_{4+} - \frac{3}{2}\xi\ell_{6+} + (8\lambda-\xi)(\ell_{7+}-\ell_{8+}) \\
&+ \frac{2\lambda^2\xi}{v^2}\ell_{8+} + 4y_1\ell_1 - 4y_2\ell_2 - 2\frac{1-2\lambda-(1-\lambda)\sqrt{\xi}}{(1-\sqrt{\xi})\sqrt{\xi}}(1-2\lambda-\xi+\lambda\sqrt{\xi})\ell_3 - 5v_1 - 5y_1 - 5v_2 + 5y_2\Big\}, \qquad (41)
\end{aligned}
$$

$$
\begin{aligned}
H_U^{4\ell} = N\Big\{&4(2-\xi)v(t_{0-}+t_{0+}) - (8+2\xi+3\xi^2)(t_{1-}+t_{1+}) - \frac{1}{2}(1+\sqrt{\xi})(2-\sqrt{\xi})^2 + 4v\ell_{4-} - 3(2-5\xi)v\ell_{5-} \\
&+ \frac{\xi}{4}(28-17\xi)\ell_{6-} + \left((6-16\lambda-13\xi)v + \frac{8\lambda^2}{v}\right)\ell_{8-} - v_\lambda\left(6-4\lambda-13\xi-2\lambda\xi + \frac{4\lambda\xi}{v_\lambda^2}(7\lambda+2\lambda^2+\xi) + \frac{8\lambda^3\xi^2}{v_\lambda^4}\right)\ell_{7-} \\
&+ v_1\left(2(y_1-3(1-\xi)) + \frac{3(1+\sqrt{\xi})^2(2+\sqrt{\xi})\sqrt{\xi}}{2(1-y_1+\sqrt{\xi})} - \frac{3(1-\sqrt{\xi})^2(2-\sqrt{\xi})\sqrt{\xi}}{2(1-y_1-\sqrt{\xi})}\right)\ell_1 - v_2\Big(2(y_2-3(1-\xi)) \\
&+ \frac{3(1+\sqrt{\xi})^2(2+\sqrt{\xi})\sqrt{\xi}}{2(1-y_2+\sqrt{\xi})} - \frac{3(1-\sqrt{\xi})^2(2-\sqrt{\xi})\sqrt{\xi}}{2(1-y_2-\sqrt{\xi})}\Big)\ell_2 - \frac{1-2\lambda-(1-\lambda)\sqrt{\xi}}{(1-2\lambda-\sqrt{\xi})\sqrt{\xi}}\{2-8\lambda+8\lambda^2-7\xi+5\lambda\xi \\
&+ 2\lambda^2\xi - 3\xi^2 - (1-6\lambda+8\lambda^2-9\xi+3\lambda\xi)\sqrt{\xi}\}\left(\frac{1}{w_1} - \frac{1}{w_2}\right) + \frac{1-2\lambda+(1-\lambda)\sqrt{\xi}}{(1-2\lambda+\sqrt{\xi})\sqrt{\xi}}\{2-8\lambda+8\lambda^2-7\xi+5\lambda\xi \\
&+ 2\lambda^2\xi - 3\xi^2 + (1-6\lambda+8\lambda^2-9\xi+3\lambda\xi)\sqrt{\xi}\}(w_1-w_2) + \frac{1}{4}(40-48\lambda-33\xi)(v_1-v_2) - 4\lambda\xi\left(\frac{v_1}{y_1} - \frac{v_2}{y_2}\right) \\
&+ \frac{b\xi\sqrt{\xi}}{2(b-aw_1)} + \frac{b\xi\sqrt{\xi}}{2(b+aw_2)} + \frac{1}{4}(24-33\xi-8v_1)y_1 - 2y_1^2 + \frac{1}{4}(24-33\xi+8v_2)y_2 - 2y_2^2\Big\}, \qquad (42)
\end{aligned}
$$

$$
\begin{aligned}
H_L^1 = N\Big\{&\xi(2-\xi)(t_{0-}-t_{0+}) - 2\xi(2+\xi)(t_{1-}-t_{1+}) - \sqrt{\xi}(1-\sqrt{\xi})(2+4\sqrt{\xi}-3\xi)t_w + \frac{1}{4}(16-54\xi+3\xi^2)v \\
&+ \xi\ell_{4+} + 16\xi\ell_{5+} + \frac{\xi}{16}(8+8\xi-3\xi^2)\ell_{6+} - \frac{\xi}{2v_\lambda^2}(8\lambda-28\lambda^2+16\lambda^3+16\lambda^4+\xi-12\lambda\xi-8\lambda^2\xi-\xi^2)\ell_{7+} \\
&- \frac{\xi}{2v^2}(8\lambda+4\lambda^2-\xi-8\lambda\xi+\xi^2)\ell_{8+} - \xi\left(2y_1 + \frac{1}{2}y_1^2\right)\ell_1 + \xi\left(2y_2 + \frac{1}{2}y_2^2\right)\ell_2 + \frac{2(1-2\lambda-(1-\lambda)\sqrt{\xi})}{(1-2\lambda-\sqrt{\xi})(1-\sqrt{\xi})\sqrt{\xi}} \\
&\times (2-8\lambda+8\lambda^2-\xi+2\lambda\xi-4\lambda^2\xi+7\xi^2-3\lambda\xi^2-(2-6\lambda+4\lambda^2+3\xi-3\lambda\xi-2\lambda^2\xi+3\xi^2)\sqrt{\xi})\ell_3 \\
&- \frac{1}{16}(32-72\xi+5\xi^2-8\xi y_1)v_1 + \frac{b\xi^2\sqrt{\xi}}{8(b-aw_1)} - \frac{1}{16}(32-72\xi+5\xi^2)y_1 - \frac{1}{16}(32-72\xi+5\xi^2-8\xi y_2)v_2 \\
&- \frac{b\xi^2\sqrt{\xi}}{8(b+aw_2)} + \frac{1}{16}(32-72\xi+5\xi^2)y_2\Big\}, \qquad (43)
\end{aligned}
$$

$$H_L^2 = \xi N\Big\{(2-\xi)(t_{0-}-t_{0+}) - 2v^2(t_{1-}-t_{1+}) - \sqrt{\xi}(1-\sqrt{\xi})t_w + \frac{1}{4}(22-3\xi)v + \ell_{4+} + \frac{1}{16}(8-8\xi+3\xi^2)\ell_{6+}$$
$$+ \frac{1}{2}(8\lambda+4\lambda^2-\xi)(\ell_{7+}-\ell_{8+}) - \frac{2\lambda^2\xi}{v^2}\ell_{8+} + \Big(2y_1+\frac{1}{2}y_1^2\Big)\ell_1 - \Big(2y_2+\frac{1}{2}y_2^2\Big)\ell_2 + 2\frac{1-2\lambda-(1-\lambda)\sqrt{\xi}}{(1-\sqrt{\xi})\sqrt{\xi}}$$
$$\times(1-2\lambda-\xi+\lambda\sqrt{\xi})\ell_3 - \frac{1}{16}(72-5\xi+8y_1)v_1 - \frac{b\xi\sqrt{\xi}}{8(b-aw_1)} - \frac{1}{16}(72-5\xi)y_1 + -\frac{1}{16}(72-5\xi+8y_2)v_2$$
$$+ \frac{b\xi\sqrt{\xi}}{8(b+aw_2)} + \frac{1}{16}(72-5\xi)y_2\Big\}, \tag{44}$$

$$H_L^{4\ell} = N\Big\{\xi(10+3\xi)(t_{1-}+t_{1+}) - \frac{\xi}{2}(24-7\xi)\ell_{6-} - 13v\xi(\ell_{5-}-\ell_{8-}) - \frac{4\lambda^2\xi}{v}\ell_{8-} - v_\lambda\Big(4\xi - \frac{8\lambda^3\xi^2}{v_\lambda^4}$$
$$+ \frac{3(1+\sqrt{\xi})^2(2+\sqrt{\xi})\sqrt{\xi}}{2(1-2\lambda+\sqrt{\xi})} - \frac{3(1-\sqrt{\xi})^2(2-\sqrt{\xi})\sqrt{\xi}}{2(1-2\lambda-\sqrt{\xi})}\Big)\ell_{7-} + -v_1\Big(4\xi + \frac{3(1+\sqrt{\xi})^2(2+\sqrt{\xi})\sqrt{\xi}}{2(1-y_1+\sqrt{\xi})}$$
$$- \frac{3(1-\sqrt{\xi})^2(2-\sqrt{\xi})\sqrt{\xi}}{2(1-y_1-\sqrt{\xi})}\Big)\ell_1 + v_2\Big(4\xi + \frac{3(1+\sqrt{\xi})^2(2+\sqrt{\xi})\sqrt{\xi}}{2(1-y_2+\sqrt{\xi})} - \frac{3(1-\sqrt{\xi})^2(2-\sqrt{\xi})\sqrt{\xi}}{2(1-y_2-\sqrt{\xi})}\Big)\ell_2$$
$$+ \frac{1-2\lambda-(1-\lambda)\sqrt{\xi}}{(1-2\lambda-\sqrt{\xi})\sqrt{\xi}}\{2-8\lambda+8\lambda^2-7\xi+5\lambda\xi+2\lambda^2\xi-3\xi^2-(1-6\lambda+8\lambda^2-9\xi+3\lambda\xi)\sqrt{\xi}\}$$
$$\times\Big(\frac{1}{w_1}-\frac{1}{w_2}\Big) + -\frac{1-2\lambda+(1-\lambda)\sqrt{\xi}}{(1-2\lambda+\sqrt{\xi})\sqrt{\xi}}\{2-8\lambda+8\lambda^2-7\xi+5\lambda\xi+2\lambda^2\xi-3\xi^2$$
$$+ (1-6\lambda+8\lambda^2-9\xi+3\lambda\xi)\sqrt{\xi}\}(w_1-w_2) + (2+7\xi)v_1 + (2+7\xi)y_1 - (2+7\xi)v_2 + (2+7\xi)y_2\Big\}, \tag{45}$$

$$H_F^{1\ell} = N\Big\{2(2-\xi)^2(t_{0-}-t_{0+}) - (8+2\xi+\xi^2)(t_{1-}-t_{1+}) + \sqrt{\xi}(1-\sqrt{\xi})(2-\sqrt{\xi})(4+\sqrt{\xi})t_w - 2(6+\xi)v$$
$$+ 2(2-\xi)\ell_{4+} + 8\xi\ell_{5+} - \frac{1}{2}(4+6\xi-3\xi^2)\ell_{6+} + \Big(16\lambda(1-\lambda^2) - 2(1+6\lambda)\xi + \xi^2 - \frac{8\lambda^2(1-2\lambda)^3}{v_\lambda^2}\Big)\ell_{7+}$$
$$- \Big(2\lambda(8-3\lambda) - 2(1+4\lambda+\lambda^2)\xi + \xi^2 - \frac{2\lambda^2}{v^2}\Big)\ell_{8+} + 4(1-2\lambda)(3-2\lambda)\ell_{9+} + 2y_1(4-3\xi-y_1)\ell_1$$
$$- 2y_2(4-3\xi-y_2)\ell_2 - \frac{2(1-2\lambda-(1-\lambda)\sqrt{\xi})}{(1-2\lambda-\sqrt{\xi})(1-\sqrt{\xi})}(6-16\lambda+8\lambda^2+11\xi-5\lambda\xi+2\lambda^2\xi-\xi^2$$
$$- (15-22\lambda+8\lambda^2+\xi+\lambda\xi)\sqrt{\xi})\ell_3 - \frac{3}{4}(4-7\xi-4y_1)v_1 + \frac{b\xi\sqrt{\xi}}{2(b-aw_1)} - \frac{1}{4}(16-21\xi)y_1 + y_1^2$$
$$- \frac{3}{4}(4-7\xi-4y_2)v_2 - \frac{b\xi\sqrt{\xi}}{2(b+aw_2)} + \frac{1}{4}(16-21\xi)y_2 - y_2^2\Big\}, \tag{46}$$

$$H_F^{2\ell} = \xi N\Big\{2(2-\xi)(t_{0-}-t_{0+}) - (4-\xi)(t_{1-}-t_{1+}) + \sqrt{\xi}(1-\sqrt{\xi})t_w + 2v + 2\ell_{4+} - \frac{3}{2}\xi\ell_{6+} + (8\lambda-\xi)(\ell_{7+}-\ell_{8+})$$
$$+ \frac{2\lambda^2\xi}{v^2}\ell_{8+} + 4y_1\ell_1 - 4y_2\ell_2 - 2\frac{1-2\lambda-(1-\lambda)\sqrt{\xi}}{(1-\sqrt{\xi})\sqrt{\xi}}(1-2\lambda-\xi+\lambda\sqrt{\xi})\ell_3 - 5v_1 - 5y_1 - 5v_2 + 5y_2\Big\}, \tag{47}$$

$$H_F^4 = N\Big\{4v(2-\xi)(t_{0-}+t_{0+}) - 2(4-5\xi)(t_{1-}+t_{1+}) - \frac{1}{2}(1+\sqrt{\xi})(2-\sqrt{\xi})^2 + 4v\ell_{4-} - 6v\ell_{5-} - 8\xi\ell_{6-}$$
$$- \frac{2}{v_\lambda}(3-14\lambda+20\lambda^2-8\lambda^3-2\xi-\xi^2)\ell_{7-} + \frac{2}{v}(3-8\lambda+4\lambda^2-2\xi+8\lambda\xi-\xi^2)\ell_{8-} + 4(1-2\lambda)(3-2\lambda)\ell_{9-}$$
$$- 2(3-y_1)v_1\ell_1 + 2(3-y_2)v_2\ell_2 + \frac{1}{4}(12+16\lambda+\xi-4y_1)v_1 + \frac{b\xi\sqrt{\xi}}{2(b-aw_1)} - \frac{4\lambda\xi v_1}{y_1} + \frac{1}{4}(24+\xi)y_1 - y_1^2$$
$$- \frac{1}{4}(12+16\lambda+\xi-4y_2)v_2 + \frac{b\xi\sqrt{\xi}}{2(b+aw_2)} + \frac{4\lambda\xi v_2}{y_2} + \frac{1}{4}(24+\xi)y_2 - y_2^2\Big\}, \tag{48}$$

$$H_I^{4T} = \frac{1}{2}\sqrt{\frac{\xi}{2}}N\Big\{2v(2-\xi)(t_{0-}+t_{0+}) - \frac{1}{2}(16+7\xi)(t_{1-}+t_{1+}) - \frac{1}{4}(1+\sqrt{\xi})(2-\sqrt{\xi})^2 + 2v\ell_{4-} + \frac{1}{8}(72-30\xi-3\xi^2)\ell_{6-}$$
$$+ v_\lambda\Big(\frac{\xi}{2} - \frac{\xi}{v_\lambda^4}(1-2\lambda-\xi)(1-4\lambda-\xi) + \frac{3(1+\sqrt{\xi})^2(2+\sqrt{\xi})}{2(1-2\lambda+\sqrt{\xi})} + \frac{3(1-\sqrt{\xi})^2(2-\sqrt{\xi})}{2(1-2\lambda-\sqrt{\xi})}\Big)\ell_{7-}$$
$$- \frac{1}{2}(12+7\xi)v(\ell_{5-}-\ell_{8-}) - \frac{1}{v}(8\lambda-4\lambda^2-\xi-8\lambda\xi-\lambda^2\xi+\xi^2)\ell_{8-} + 2(1-2\lambda)\ell_{9-}$$
$$+ v_1\Big(\frac{\xi}{2} + \frac{3(1+\sqrt{\xi})^2(2+\sqrt{\xi})}{2(1-y_1+\sqrt{\xi})} + \frac{3(1-\sqrt{\xi})^2(2-\sqrt{\xi})}{2(1-y_1-\sqrt{\xi})}\Big)\ell_1 - v_2\Big(\frac{\xi}{2} + \frac{3(1+\sqrt{\xi})^2(2+\sqrt{\xi})}{2(1-y_2+\sqrt{\xi})} + \frac{3(1-\sqrt{\xi})^2(2-\sqrt{\xi})}{2(1-y_2-\sqrt{\xi})}\Big)\ell_2$$
$$+ \frac{1-2\lambda-(1-\lambda)\sqrt{\xi}}{(1-2\lambda-\sqrt{\xi})\xi}\{2-8\lambda+8\lambda^2-7\xi+5\lambda\xi+2\lambda^2\xi-3\xi^2-(1-6\lambda+8\lambda^2-9\xi+3\lambda\xi)\sqrt{\xi}\}\Big(\frac{1}{w_1}-\frac{1}{w_2}\Big)$$
$$+ \frac{1-2\lambda+(1-\lambda)\sqrt{\xi}}{(1-2\lambda+\sqrt{\xi})\xi}\{2-8\lambda+8\lambda^2-7\xi+5\lambda\xi+2\lambda^2\xi-3\xi^2+(1-6\lambda+8\lambda^2-9\xi+3\lambda\xi)\sqrt{\xi}\}(w_1-w_2)$$
$$- \frac{1}{8}(28+5\xi)v_1 - \frac{2\lambda\xi v_1}{y_1} + \frac{b\xi\sqrt{\xi}}{4(b-aw_1)} - \frac{1}{8}(28+5\xi)y_1 + \frac{1}{8}(28+5\xi)v_2 + \frac{2\lambda\xi v_2}{y_2} + \frac{b\xi\sqrt{\xi}}{4(b+aw_2)} - \frac{1}{8}(28+5\xi)y_2\Big\}, \tag{49}$$

$$H_A^{1T} = \frac{1}{2}\sqrt{\frac{\xi}{2}}N\Big\{2(2-\xi)(t_{0-}-t_{0+}) - \frac{1}{2}(16-3\xi)(t_{1-}-t_{1+}) - \frac{1}{2}(1-\sqrt{\xi})(2-\sqrt{\xi})(4+\sqrt{\xi})t_w - \frac{1}{2}(16-3\xi)v + 2\ell_{4+}$$
$$+ 2(7-\xi)\ell_{5+} - \frac{1}{8}(8-6\xi+3\xi^2)\ell_{6+} + 2(1-2\lambda)\ell_{9+} + \frac{\xi}{2}y_1\ell_1 - \frac{\xi}{2}y_2\ell_2 - \xi\Big(1-\lambda-\frac{4\lambda^2}{v_\lambda^2}\Big)\ell_{7+}$$
$$- \Big(4\lambda(2-\lambda) - \xi + \frac{\lambda^2\xi}{v}\Big)\ell_{8+} + \frac{1-2\lambda-(1-\lambda)\sqrt{\xi}}{(1-\sqrt{\xi})\sqrt{\xi}}(6-4\lambda-(9-\xi)\sqrt{\xi}+(2-\lambda)\xi - \frac{8\lambda^2\sqrt{\xi}}{1-2\lambda-\sqrt{\xi}}\Big)\ell_3$$
$$- \frac{1}{8}(4+5\xi)v_1 + \frac{b\xi\sqrt{\xi}}{4(b-aw_1)} - \frac{1}{8}(4+5\xi)y_1 - \frac{1}{8}(4+5\xi)v_2 - \frac{b\xi\sqrt{\xi}}{4(b+aw_2)} + \frac{1}{8}(4+5\xi)y_2\Big\}, \tag{50}$$

$$H_A^{2T} = \frac{1}{2}\sqrt{\frac{\xi}{2}}N\Big\{2(2-\xi)(t_{0-}-t_{0+}) - \frac{1}{2}(8-3\xi)(t_{1-}-t_{1+}) - \frac{\xi}{2}(1-\sqrt{\xi})t_w + \frac{3}{2}(4-\xi)v + 2\ell_{4+} + 2(1+\xi)\ell_{5+}$$
$$+ \frac{1}{8}(2-\xi)(4-3\xi)\ell_{6+} + (8\lambda-\xi-\lambda\xi)\ell_{7+} - \Big(4\lambda(2+\lambda) - \xi + \frac{\lambda^2\xi}{v}\Big)\ell_{8+} - 2(1-2\lambda)\ell_{9+}$$
$$+ \frac{1}{2}(8-\xi)y_1\ell_1 - \frac{1}{2}(8-\xi)y_2\ell_2 + \frac{1-2\lambda-(1-\lambda)\sqrt{\xi}}{1-\sqrt{\xi}}(1-2\lambda+\lambda\sqrt{\xi}-\xi)\ell_3 - \frac{1}{8}(52-5\xi)v_1$$
$$- \frac{b\xi\sqrt{\xi}}{4(b-aw_1)} - \frac{1}{8}(52-5\xi)y_1 - \frac{1}{8}(52-5\xi)v_2 + \frac{b\xi\sqrt{\xi}}{4(b+aw_2)} + \frac{1}{8}(52-5\xi)y_2\Big\}, \tag{51}$$

$$H_A^{3N} = \frac{1}{2}\sqrt{\frac{\xi}{2}}N\Big\{2v(2-\xi)(t_{0-}+t_{0+}) - \frac{1}{2}(8-13\xi)(t_{1-}+t_{1+}) + \frac{1}{4}(2-\sqrt{\xi})^2(1+\sqrt{\xi}) + 2v\ell_{4-} - \frac{1}{2}(8+\xi)v\ell_{5-}$$
$$+ \frac{1}{8}(8-30\xi+3\xi^2)\ell_{6-} - \Big(\frac{8+\xi}{2}v_\lambda - \xi\frac{1-2\lambda-\xi}{v_\lambda}\Big)\ell_{7-} + v\Big(4(1-\lambda)^2 + \frac{3}{2}\xi - \frac{3\lambda^2\xi}{v^2}\Big)\ell_{8-}$$
$$- 2(1-2\lambda)\ell_{9-} - \frac{1}{2}(8+\xi)v_1\ell_1 + \frac{1}{2}(8+\xi)v_2\ell_2 + \frac{1}{8}(52+5\xi)v_1 - \frac{2\lambda\xi v_1}{y_1} - \frac{b\xi\sqrt{\xi}}{4(b-aw_1)}$$
$$+ \frac{1}{8}(52+5\xi)y_1 - \frac{1}{8}(52+5\xi)v_2 + \frac{2\lambda\xi v_2}{y_2} - \frac{b\xi\sqrt{\xi}}{4(b+aw_2)} + \frac{1}{8}(52+5\xi)y_2\Big\}. \tag{52}$$

The logarithmic rate terms ℓ_i and the double and dilogarithmic rate terms t_{0-}, t_{0+}, t_{1-}, t_{1+}, and t_w are listed in Appendix C. Note the exact $O(\alpha_s)$ tree graph relation $H_F^{2\ell} = H_U^2$ which was also noticed in [11]. We have not been able to derive this relation from general principles.

We shall not dwell on the technical details of how the finite integrals have been calculated but rather concentrate on the class of IR-divergent integrals. For instance, the integral

$$\tilde{I}_z(-1,-1) = \int_0^{y_1}\int_{z_-}^{z_+}\frac{dydz}{yz} = \int_0^{y_1}\ln\Big(\frac{z_+(y)}{z_-(y)}\Big)\frac{dy}{y} \tag{53}$$

is IR divergent and will be regularized by a gluon mass $m_G = \sqrt{\Lambda q^2}$. The introduction of a gluon mass changes the lower y limit from 0 to $y_- = \Lambda + \sqrt{\Lambda\xi}$, and the z limits to

$$z_\pm(y) = \frac{1}{4y+\xi}(2y - 2y^2 - \xi y + 2\Lambda y + 2\Lambda$$
$$\pm 2\sqrt{(y-\Lambda)^2 - \Lambda\xi}\sqrt{(1-y)^2 - \xi}). \tag{54}$$

Therefore, the integration over z gives rise to

$$\tilde{I}_z(-1,-1) = \int_{y_-}^{y_1}\ln\Big(\frac{2y-2y^2-\xi y+2\Lambda y+2\Lambda+2\sqrt{(y-\Lambda)^2-\Lambda\xi}\sqrt{(1-y)^2-\xi}}{2y-2y^2-\xi y+2\Lambda y+2\Lambda-2\sqrt{(y-\Lambda)^2-\Lambda\xi}\sqrt{(1-y)^2-\xi}}\Big)\frac{dy}{y}. \tag{55}$$

This integral is not analytically calculable for general values of Λ. However, we can divide the integral into a divergent and a convergent part which are separately calculable as long as Λ is a small parameter. The residue of the divergent part should coincide with the residue of the original integrand at the IR singular pole at $y = 0$. A simplified IR-divergent part can be constructed from the full integrand by neglecting higher powers in y whenever possible. Before this approximation we shift the integration by $-\Lambda$ in order to facilitate the expansion around the lower boundary. We obtain

$$\tilde{I}_z^D(-1,-1) = \int_{\sqrt{\Lambda\xi}}^{y_1}\ln\Big(\frac{(1+v^2)y + 2v\sqrt{y^2-\Lambda\xi}}{(1+v^2)y - 2v\sqrt{y^2-\Lambda\xi}}\Big)\frac{dy}{y}. \tag{56}$$

This integral can be calculated analytically and one obtains

$$\tilde{I}_z^D(-1,-1) = \ln\Big(\frac{1+v}{1-v}\Big)\ln\Big(\frac{y_1^2}{\Lambda\xi}\Big) - \mathrm{Li}_2\Big(\frac{2v}{(1+v)^2}\Big)$$
$$+ \mathrm{Li}_2\Big(\frac{-2v}{(1-v)^2}\Big) - \frac{1}{2}\mathrm{Li}_2\Big(-\frac{(1+v)^2}{(1-v)^2}\Big)$$
$$+ \frac{1}{2}\mathrm{Li}_2\Big(-\frac{(1-v)^2}{(1+v)^2}\Big)$$
$$=: t_p - \ln\Big(\frac{1+v}{1-v}\Big)\ln\Lambda. \tag{57}$$

In the case $\Lambda \to 0$ we have the limiting value (we write $\varepsilon = \sqrt{\Lambda\xi}$)

$$\tilde{I}_z^D(-1,-1) \to 2\ln\Big(\frac{1+v}{1-v}\Big)\lim_{\varepsilon\to 0}\int_\varepsilon^{y_1}\frac{dy}{y} \tag{58}$$

which is an ill-defined quantity for $\varepsilon = 0$. However, we can subtract the singular piece from the original integral also taken in the limit $\Lambda \to 0$. As a result the divergences cancel and one obtains

$$\tilde{I}_z^C(-1,-1) = \lim_{\varepsilon\to 0}\Big\{\int_\varepsilon^{y_1}\ln\Big(\frac{2-2y-\xi+2\sqrt{(1-y)^2-\xi}}{2-2y-\xi-2\sqrt{(1-y)^2-\xi}}\Big)$$
$$\times\frac{dy}{y} - 2\ln\Big(\frac{1+v}{1-v}\Big)\int_\varepsilon^{y_1}\frac{dy}{y}\Big\} \tag{59}$$

or symbolically

$$\tilde{I}_z^C(-1,-1) = \lim_{\varepsilon\to 0}\Big\{\hat{I}_z^{bal\prime}(-1) - 2\ln\Big(\frac{1+v}{1-v}\Big)\hat{I}_z^{l\prime}(-1)\Big\}, \tag{60}$$

where the primes indicates that the lower limit is ε. With the Euler substitution Eq. (39), and after partial fractioning according to

$$\frac{dy}{y} = -\frac{dw}{w_0-w} + \frac{dw}{w_0+w} + \frac{dw}{1-w} - \frac{dw}{1+w} \tag{61}$$

one obtains

$$\hat{I}_z^{bat}(-1) = \int_\varepsilon^{y_1} \ln\!\left(\frac{2-2y-\xi+2\sqrt{(1-y)^2-\xi}}{2-2y-\xi-2\sqrt{(1-y)^2-\xi}}\right)\frac{dy}{y}$$
$$= I_{0-}^{ba}(w_0') - I_{0-}^{ba}(w_1) - I_{0+}^{ba}(w_0') + I_{0+}^{ba}(w_1)$$
$$- I_{1-}^{ba}(w_0') + I_{1-}^{ba}(w_1) + I_{1+}^{ba}(w_0') - I_{1+}^{ba}(w_1), \tag{62}$$

$$\hat{I}_z^{l}(-1) = \int_\varepsilon^{y_1} \frac{dy}{y}$$
$$= I_{0-}(w_0') - I_{0-}(w_1) - I_{0+}(w_0') + I_{0+}(w_1)$$
$$- I_{1-}(w_0') + I_{1-}(w_1) + I_{1+}(w_0') - I_{1+}(w_1), \tag{63}$$

where

$$w_0' = \sqrt{\frac{1-\varepsilon-\sqrt{\xi}}{1-\varepsilon+\sqrt{\xi}}} = w_0\left(1 - \frac{\varepsilon\sqrt{\xi}}{1-\xi} + \cdots\right). \tag{64}$$

The variable w_0' tends to w_0 for $\varepsilon \to 0$. It is instructive to note that the divergences now reside in the terms $I_{0-}^{ba}(w_0')$ and $I_{0-}(w_0')$ which contain the integrand factor $(w_0 - w)^{-1}$. We obtain

$$I_{0-}^{ba}(w) = t_p^l(w) - 2\ln\!\left(\frac{1+v}{1-v}\right)\ln(w_0 - w),$$
$$I_{0-}(w) = -\ln(w_0 - w), \tag{65}$$

where t_p^l is a decay rate term which vanishes in the limit $w \to w_0$. For this reason the two expressions in Eq. (65) do not contribute to the convergent part at all. Using Eqs. (62) and (63) we can calculate the convergent part in Eq. (60) and add the divergent part in Eq. (57) to obtain

$$\tilde{I}_z(-1,-1) = t_p - \ln\!\left(\frac{1+v}{1-v}\right)\ln\Lambda$$
$$- \left\{I_{0-}^{ba}(w_1) - 2\ln\!\left(\frac{1+v}{1-v}\right)I_{0-}(w_1)\right\} + \cdots$$
$$= t_{0-}^{ba}(w_0) - t_{0-}^{ba}(w_1) - t_{0+}^{ba}(w_0) + t_{0+}^{ba}(w_1)$$
$$+ \cdots - \ln\!\left(\frac{1+v}{1-v}\right)\ln\Lambda. \tag{66}$$

The dots indicate further contributions according to Eqs. (62) and (63) where we can replace w_0' by w_0. The decay rate terms $t_{0-}^{ba}(w), t_{0+}^{ba}(w), \ldots$ are listed in Appendix C. It is obvious that $t_{0-}^{ba}(w_0)$ in Eq. (66) has to be replaced by the special value t_p defined in Eq. (57).

We now turn to case B when $\lambda > \lambda_{\text{trans}}$. As discussed in the beginning of this section this entails the calculation of the second integral in Eq. (36) which has to be added to the first and the third integral in Eq. (36). The latter two integrals are already known from case A. Using some additional decay rate terms listed in Appendix C the results for this additional phase-space portion are given by

$$H_U^1 = N\Big\{2(2-\xi)^2(t_{0-}^c - t_{0+}^c) - (8-10\xi-\xi^2)(t_{1-}^c - t_{1+}^c)$$
$$+ \sqrt{\xi}(1-\sqrt{\xi})(2+4\sqrt{\xi}-3\xi)t_w^c - 8(2-\xi)v\ell_{4+}^c$$
$$- 16\xi\ell_{5+}^c + \left(\frac{1}{4}(8+12\xi-\xi^2) + 8y_2 - 2y_2^2\right)\ell_2^c$$
$$+ \frac{1}{2}(24+5\xi)v_2 - \frac{\xi(4-\xi)v_2}{2(4y_2+\xi)}\Big\}, \tag{67}$$

$$H_U^2 = \xi N\Big\{2(2-\xi)(t_{0-}^c - t_{0+}^c) - (4-\xi)(t_{1-}^c - t_{1+}^c)$$
$$+ \sqrt{\xi}(1-\sqrt{\xi})t_w^c - 8v\ell_{4+}^c + \left(\frac{3}{2}\xi + 4y_2\right)\ell_2^c + 10v_2\Big\}, \tag{68}$$

$$H_U^{4\ell} = N\Big\{4(2-\xi)v(t_{0-}^c + t_{0+}^c) - (8+2\xi+3\xi^2)(t_{1-}^c + t_{1+}^c) - 8(1-\xi)\ell_{4-}^c + 16(1-\xi)\ell_{5-}^c$$
$$- \frac{\xi}{4}(28-17\xi)(2\ell_{5-}^c + \ell_{6-}^c) - 16(1-\xi)\ell_{7-}^c + v_2\Big(2(y_2 - 3(1-\xi)) + \frac{3(1+\sqrt{\xi})^2(2+\sqrt{\xi})\sqrt{\xi}}{2(1-y_2+\sqrt{\xi})}$$
$$- \frac{3(1-\sqrt{\xi})^2(2-\sqrt{\xi})\sqrt{\xi}}{2(1-y_2-\sqrt{\xi})}\Big)\ell_2^c + \frac{1}{8}(64+64\sqrt{\xi}-352\xi+232\xi\sqrt{\xi}+\xi^2) - \frac{3}{2}(8-11\xi)y_2 + 4y_2^2 - \frac{\xi(4-\xi)^2}{8(4y_2+\xi)}\Big\}, \tag{69}$$

$$H_L^1 = N\Big\{\xi(2-\xi)(t_{0-}^c - t_{0+}^c) - 2\xi(2+\xi)(t_{1-}^c - t_{1+}^c) - \sqrt{\xi}(2+2\sqrt{\xi}-7\xi+3\xi\sqrt{\xi})t_w^c - 4\xi v\ell_{4+}^c + 16\xi\ell_{5+}^c$$
$$- \xi\left(\frac{1}{16}(8+8\xi-3\xi^2) + 2y_2 + \frac{1}{2}y_2^2\right)\ell_2^c + \frac{1}{8}(32-72\xi+5\xi^2-8\xi y_2)v_2 - \frac{\xi^2(4-\xi)v_2}{8(4y_2+\xi)}\Big\}, \tag{70}$$

$$H_L^2 = \xi N\Big\{(2-\xi)(t_{0-}^c - t_{0+}^c) - 2(1-\xi)(t_{1-}^c - t_{1+}^c) - \sqrt{\xi}(1-\sqrt{\xi})t_w^c - 4v\ell_{4+}^c - \Big(\frac{1}{16}(8-8\xi+3\xi^2) - 2y_2 - \frac{1}{2}y_2^2\Big)\ell_2^c + \frac{1}{8}(72-5\xi+8y_2)v_2 + \frac{\xi(4-\xi)v_2}{8(4y_2+\xi)}\Big\}, \tag{71}$$

$$H_L^{4\ell} = N\Big\{\xi(10+3\xi)(t_{1-}^c + t_{1+}^c) + \xi(24-7\xi)\ell_{5-}^c + \frac{1}{2}\xi(24-7\xi)\ell_{6-}^c + \Big(\frac{3\sqrt{\xi}}{2w_2}(2-\sqrt{\xi})(1-\sqrt{\xi})^2 - \frac{3\sqrt{\xi}w_2}{2}(2+\sqrt{\xi})(1+\sqrt{\xi})^2 - 4\xi v_2\Big)\ell_2^c + 2(1-\sqrt{\xi})(2-6\sqrt{\xi}+13\xi) - 2(2+7\xi)y_2\Big\}, \tag{72}$$

$$H_F^{1\ell} = N\Big\{2(2-\xi)^2(t_{0-}^c - t_{0+}^c) - (8+2\xi+\xi^2)(t_{1-}^c - t_{1+}^c) + \sqrt{\xi}(8-10\sqrt{\xi}+\xi+\xi\sqrt{\xi})t_w^c - 8(2-\xi)v\ell_{4+}^c + 8\xi\ell_{5+}^c + \Big(\frac{1}{2}(4+6\xi-3\xi^2) + 2(4-3\xi)y_2 - 2y_2^2\Big)\ell_2^c + \frac{3}{2}(4-7\xi-4y_2)v_2 - \frac{\xi(4-\xi)v_2}{2(4y_2+\xi)}\Big\}, \tag{73}$$

$$H_F^{2\ell} = \xi N\Big\{2(2-\xi)(t_{0-}^c - t_{0+}^c) - (4-\xi)(t_{1-}^c - t_{1+}^c) + \sqrt{\xi}(1-\sqrt{\xi})t_w^c - 8v\ell_{4+} + \Big(\frac{3}{2}\xi + 4y_2\Big)\ell_2^c + 10v_2\Big\}, \tag{74}$$

$$H_F^4 = N\Big\{4(2-\xi)v(t_{0-}^c + t_{0+}^c) - 2(4-5\xi)(t_{1-}^c + t_{1+}^c) - 8(1-\xi)\ell_{4-}^c + 16\ell_{5-}^c + 8\xi\ell_{6-}^c - 16(1-\xi)\ell_{7-}^c - 2(3-y_2)v_2\ell_2^c + \frac{1}{8}(80-64\sqrt{\xi}-8\xi+\xi^2) - \frac{1}{2}(24+\xi)y_2 + 2y_2^2 - \frac{\xi(4-\xi)^2}{8(4y_2+\xi)}\Big\}, \tag{75}$$

$$H_I^{4T} = \frac{1}{2}\sqrt{\frac{\xi}{2}}N\Big\{2(2-\xi)v(t_{0-}^c + t_{0+}^c) - \frac{1}{2}(16+7\xi)(t_{1-}^c + t_{1+}^c) - 4(1-\xi)\ell_{4-}^c - \frac{1}{4}(4-\xi)(10+3\xi)\ell_{5-}^c - \frac{1}{8}(72-30\xi-3\xi^2)\ell_{6-}^c - 8(1-\xi)\ell_{7-}^c + \Big(\frac{\xi v_2}{2} + \frac{3}{2w_2}(2-\sqrt{\xi})(1-\sqrt{\xi})^2 + \frac{3w_2}{2}(2+\sqrt{\xi})(1+\sqrt{\xi})^2\Big)\ell_2^c - \frac{1}{16}(304-496\sqrt{\xi}+208\xi-24\xi\sqrt{\xi}-\xi^2) + \frac{1}{4}(28+5\xi)y_2 - \frac{\xi(4-\xi)^2}{16(4y_2+\xi)}\Big\}, \tag{76}$$

$$H_A^{1T} = \frac{1}{2}\sqrt{\frac{\xi}{2}}N\Big\{2(2-\xi)(t_{0-}^c - t_{0+}^c) - \frac{1}{2}(16-3\xi)(t_{1-}^c - t_{1+}^c) - \frac{1}{2}(8-10\sqrt{\xi}+\xi+\xi\sqrt{\xi})t_w^c - 8v\ell_{4+}^c + 2(7-\xi)\ell_{5+}^c + \Big(\frac{1}{8}(8-6\xi+3\xi^2) + \frac{1}{2}\xi y_2\Big)\ell_2^c + \frac{1}{4}(4+5\xi)v_2 - \frac{\xi(4-\xi)v_2}{4(4y_2+\xi)}\Big\}, \tag{77}$$

$$H_A^{2T} = \frac{1}{2}\sqrt{\frac{\xi}{2}}N\Big\{2(2-\xi)(t_{0-}^c - t_{0+}^c) - \frac{1}{2}(8-3\xi)(t_{1-}^c - t_{1+}^c) - \frac{1}{2}\xi(1-\sqrt{\xi})t_w^c - 8v\ell_{4+}^c + 2(1+\xi)\ell_{5+}^c - \Big(\frac{1}{8}(2-\xi)(4-3\xi) - \frac{1}{2}(8-\xi)y_2\Big)\ell_2^c + \frac{1}{4}(52-5\xi)v_2 + \frac{\xi(4-\xi)v_2}{4(4y_2+\xi)}\Big\}, \tag{78}$$

$$H_A^{3N} = \frac{1}{2}\sqrt{\frac{\xi}{2}}N\Big\{2(2-\xi)v(t_{0-}^c + t_{0+}^c) - \frac{1}{2}(8-13\xi)(t_{1-}^c + t_{1+}^c) - 4(1-\xi)\ell_{4-}^c + \frac{1}{4}(24-2\xi-3\xi^2)\ell_{5-}^c - \frac{1}{8}(8-30\xi+3\xi^2)\ell_{6-}^c - 8(1-\xi)\ell_{7-}^c - \frac{1}{2}(8+\xi)v_2\ell_2^c + \frac{1}{16}(208-208\sqrt{\xi}+16\xi-24\xi\sqrt{\xi}-\xi^2) - \frac{1}{4}(52+5\xi)y_2 + \frac{\xi(4-\xi)^2}{4(4y_2+\xi)}\Big\}. \tag{79}$$

Note again that one has the remarkable relation $H_F^{2\ell} = H_U^2$. We mention that, differing from Ref. [12], we have been able to obtain a closed form result for the cut-dependent structure function H_F^4 [see Eqs. (48) and (75)].

Numerically, the contribution of the second integral in Eq. (36) calculated above is quite small. This is because the relevant integration region is far away from the IR region where the rate is largest. Nevertheless, this contribution is needed if one wants to check on the consistency of our case B result with the fully integrated results in Refs. [7–11]. In fact, we have performed an explicit check that for each of the unpolarized and polarized rate functions the sum of the three integrals in Eq. (36) reproduces the full phase-space result calculated previously in Refs. [7–11] when the gluon energy cut is set to its maximal value $\lambda_{\max} = (1-\xi)/2$ [which corresponds to setting y_1 and y_2 to $(1-\xi)/2$ in Eq. (36)]. We have also checked that our exact result converges to the soft-gluon expression to be derived in Sec. VI when $\lambda \to 0$.

V. FULLY INTEGRATED $O(\alpha_s)$ RESULTS

The cutoff dependent helicity structure functions calculated in the previous section must coincide with the fully integrated results written down in Refs. [8–10] when the cutoff is taken to its maximal value. For the convenience of the reader we collect the fully integrated results of [8–10] and list them in terms of the sum $H_a^{j(m)}(\alpha_s) = H_a^{j(m)}(\text{tree}) + H_a^{j(m)}(\text{loop})$. As before we define [$N = \alpha_s N_c C_F q^2/(4\pi v)$]. One has

$$
\begin{aligned}
H_U^1(\alpha_s) &= N\Big\{(2+7\xi)v + \frac{1}{2}(48-48\xi+7\xi^2)t_3 + \sqrt{\xi}(2-7\xi)t_4 + \xi(2+3\xi)(t_4-t_5) - 2(2-\xi)((2-\xi)(t_8-t_9) \\
&\quad + 2v(t_{10}+2t_{12}))\Big\}, \\
H_U^2(\alpha_s) &= \xi N\{6v + (6-\xi)t_3 + \sqrt{\xi}t_4 - \xi(t_4-t_5) - 2((2-\xi)(t_8-t_9) + 2v(t_{10}+2t_{12}))\}, \\
H_L^1(\alpha_s) &= N\Big\{\frac{1}{4}(16-46\xi+3\xi^2)v + \frac{\xi}{8}(88-32\xi+3\xi^2)t_3 - \sqrt{\xi}(2-7\xi)t_4 - \xi(2+3\xi)(t_4-t_5) \\
&\quad - \xi((2-\xi)(t_8-t_9) + 2v(t_{10}+2t_{12}))\Big\}, \\
H_L^2(\alpha_s) &= \xi N\Big\{\frac{3}{4}(10-\xi)v + \frac{1}{8}(24-16\xi-3\xi^2)t_3 - \sqrt{\xi}t_4 + \xi(t_4-t_5) - ((2-\xi)(t_8-t_9) + 2v(t_{10}+2t_{12}))\Big\}, \\
H_F^3(\alpha_s) &= -4\xi N v\pi, \\
H_F^4(\alpha_s) &= N\{-8\sqrt{\xi}(1-\sqrt{\xi}) - 8(t_1-t_2) + 4(2-3\xi)vt_3 - 2(4-5\xi)t_6 - 4v((2-\xi)(t_8-t_7) + 2v(t_{10}+t_{11}))\},
\end{aligned}
\tag{80}
$$

$$
\begin{aligned}
H_U^{3\ell}(\alpha_s) &= -4\xi N v\pi, \\
H_U^{4\ell}(\alpha_s) &= N\Big\{-(2+35\xi) + \sqrt{\xi}(8+29\xi) - \frac{1}{4}(32-60\xi+17\xi^2)(t_1-t_2) + 2(4+9\xi)vt_3 - (8+2\xi+3\xi^2)t_6 \\
&\quad - 4v((2-\xi)(t_8-t_7) + v(t_{10}+t_{11}))\Big\}, \\
H_L^{3\ell}(\alpha_s) &= 0, \\
H_L^{4\ell}(\alpha_s) &= N\Big\{2(2+19\xi) - 2\sqrt{\xi}(8+13\xi) - \frac{1}{2}\xi(24-7\xi)(t_1-t_2) - 26\xi vt_3 + \xi(10+3\xi)t_6\Big\}, \\
H_F^{1\ell}(\alpha_s) &= N\{-2(2+3\xi)v + (24-12\xi+\xi^2)t_3 + \sqrt{\xi}(8+\xi)t_4 - \xi(10-\xi)(t_4-t_5) \\
&\quad - 2(2-\xi)((2-\xi)(t_8-t_9) + 2v(t_{10}+2t_{12}))\}, \\
H_F^{2\ell}(\alpha_s) &= \xi N\{6v + (6-\xi)t_3 + \sqrt{\xi}t_4 - \xi(t_4-t_5) - 2((2-\xi)(t_8-t_9) + 2v(t_{10}+2t_{12}))\},
\end{aligned}
\tag{81}
$$

$$H_I^{3T}(\alpha_s) = -\frac{1}{2}\sqrt{\frac{\xi}{2}}N(1+\xi)v\pi,$$

$$H_I^{4T}(\alpha_s) = -\frac{1}{4}\sqrt{\frac{\xi}{2}}N\Big\{48+17\xi-\sqrt{\xi}(62+3\xi)-\frac{1}{4}(4-\xi)(10+3\xi)(t_1-t_2)-2(21+2\xi)vt_3$$
$$+(16+7\xi)t_6+4v((2-\xi)(t_8-t_7)+2v(t_{10}+t_{11}))\Big\},$$

$$H_A^{1T}(\alpha_s) = -\frac{1}{4}\sqrt{\frac{\xi}{2}}N\Big\{(8-3\xi)v-\frac{1}{2}(72-38\xi+3\xi^2)t_3-\sqrt{\xi}(10-\xi)t_4+(8+\xi)(t_4-t_5)$$
$$+4((2-\xi)(t_8-t_9)+2v(t_{10}+2t_{12}))\Big\},$$

$$H_A^{2T}(\alpha_s) = -\frac{1}{4}\sqrt{\frac{\xi}{2}}N\Big\{-(20-3\xi)v-\frac{1}{2}(32-14\xi-3\xi^2)t_3-\xi\sqrt{\xi}t_4+\xi(t_4-t_5)+4((2-\xi)(t_8-t_9)+2v(t_{10}+2t_{12}))\Big\}, \tag{82}$$

$$H_I^{1N}(\alpha_s) = \frac{1}{2}\sqrt{\frac{\xi}{2}}Nv^2\pi = H_I^{2N}(\alpha_s),$$

$$H_A^{3N}(\alpha_s) = \frac{1}{4}\sqrt{\frac{\xi}{2}}N\Big\{20+9\xi-\sqrt{\xi}(26+3\xi)-\frac{1}{4}(24-2\xi-3\xi^2)(t_1-t_2)+2(1-6\xi)vt_3$$
$$-(8-13\xi)t_6-4v((2-\xi)(t_8-t_7)+2v(t_{10}+t_{11}))\Big\},$$

$$H_A^{4N}(\alpha_s) = \frac{1}{2}\sqrt{\frac{\xi}{2}}N(1+\xi)v\pi. \tag{83}$$

The fully integrated $O(\alpha_s)$ results are given in terms of the rate functions t_1 to t_{12} which are listed in Appendix B. It is clear that one again has the relation $H_F^{2\ell}(\alpha_s) = H_U^2(\alpha_s)$ because both loop and tree contributions satisfy this identity.

VI. THE SOFT-GLUON APPROXIMATION

The basic ingredient of the SGA for the tree graph matrix elements is the eikonal approximation where the gluon momentum is neglected in the numerators of Feynman diagram contributions. In the eikonal approximation the hadron tensor is proportional to the Born term. In the present case one has

$$H^i_{\mu\nu}(\text{soft}) = g_s^2 C_F\Big(\frac{p_1^2}{(p_1p_3)^2}-\frac{2(p_1p_2)}{(p_1p_3)(p_2p_3)}+\frac{p_2^2}{(p_2p_3)^2}\Big)H^i_{\mu\nu}(\text{Born}), \tag{84}$$

where $H^i_{\mu\nu}(\text{Born})$ refers to the Born term tensor in the two-body case where $q = p_1 + p_2$. On the other hand, the eikonal factor multiplying $H^i_{\mu\nu}(\text{Born})$ refers to the three-body case where $q = p_1 + p_2 + p_3$ and depends on the dimensionless three-body phase-space variables $x = E_G/\sqrt{q^2} = p_3q/q^2$ and $u = (p_1 - p_2)q/q^2$. When integrating $H^i_{\mu\nu}(\text{soft})$ over the three-body phase space the Born term contribution $H^i_{\mu\nu}(\text{Born})$ can be taken outside of the integral. In this sense the integration on the soft-gluon factor in Eq. (84) is universal in the sense that it is process and polarization independent.

When projecting the eikonal contribution in Eq. (84) onto the various helicity structure functions one recovers the various Born term contributions $H^i_a(\text{Born})$ listed in Sec. III. Referring to the integration measure in Eq. (14) and using $dydz = 2dxdu$ one obtains

$$\frac{2q^2}{16\pi^2 v}\int_{\sqrt{\Lambda}}^{\lambda}\int_{-u_+}^{u_+} H^i_{\mu\nu}(\text{soft})dxdu = H^i_{\mu\nu}(\text{Born})\frac{\alpha_s C_F}{4\pi v}\int_{\sqrt{\Lambda}}^{\lambda}\int_{-u_+}^{u_+} h(x,u)dxdu, \tag{85}$$

where

$$h(x,u) = 8\frac{(1-2x+\Lambda)(u^2-(x-\Lambda)^2)+\xi(x-\Lambda)^2}{(u^2-(x-\Lambda)^2)^2}. \tag{86}$$

The limits of the u integration are given by $\pm u_+$ where

$$u_+(x) = \left((x^2 - \Lambda)\frac{1 - 2x + \Lambda - \xi}{1 - 2x + \Lambda}\right)^{1/2}. \quad (87)$$

After integration over u one obtains

$$h(x) = -4\left(\frac{-2u_+\xi}{(x-\Lambda)^2 - u_+^2} + \frac{2 - 4x - 2\Lambda - \xi}{x - \Lambda} \times \ln\left(\frac{x - \Lambda + u_+}{x - \Lambda - u_+}\right)\right). \quad (88)$$

Further integrating over the scaled gluon energy x from Λ to λ one finally has

$$h_{\rm eik} = -\frac{\alpha_s C_F}{\pi v}\left\{\left(2v - (2-\xi)\ln\left(\frac{1+v}{1-v}\right)\right)\ln\left(\frac{2\lambda}{\sqrt{\Lambda}}\right) + 4(\sqrt{1-2\lambda}\sqrt{1-2\lambda-\xi} - v) + 2\left(\ln\left(\frac{z_\lambda}{z_0}\right) + 2\ln\left(\frac{z_0^2 - 1}{z_\lambda z_0 - 1}\right)\right) - \ln z_0 + 4\lambda \ln z_\lambda + (2-\xi) \times \left(\frac{1}{2}\ln^2\left(\frac{z_\lambda}{z_0}\right) + 2\ln z_0 \ln\left(\frac{z_\lambda z_0 - 1}{z_0^2 - 1}\right) + \frac{1}{4}\ln^2 z_0 + {\rm Li}_2\left(\frac{2v}{1+v}\right) + {\rm Li}_2\left(1 - \frac{z_\lambda}{z_0}\right) + {\rm Li}_2(1 - z_\lambda z_0) - {\rm Li}_2(1 - z_0^2)\right)\right\}, \quad (89)$$

where

$$z_0 = \frac{1+v}{1-v}, \qquad z_\lambda = \frac{\sqrt{1-2\lambda} + \sqrt{1-2\lambda-\xi}}{\sqrt{1-2\lambda} - \sqrt{1-2\lambda-\xi}}. \quad (90)$$

The function $h_{\rm eik}$ will be referred to as the eikonal form of the SGA factor.

For $\lambda \to 0$ one obtains

$$h_{\rm SGA} = -\frac{\alpha_s C_F}{\pi v}\left\{\left(2v - (2-\xi)\ln\left(\frac{1+v}{1-v}\right)\right)\ln\left(\frac{2\lambda}{\sqrt{\Lambda}}\right) - \ln\frac{1+v}{1-v} + (2-\xi)\left(\frac{1}{4}\ln^2\left(\frac{1+v}{1-v}\right) + {\rm Li}_2\left(\frac{2v}{1+v}\right)\right)\right\}. \quad (91)$$

Following the literature [14,16] we shall refer to the SGA factor (91) as the soft-gluon approximation of Eq. (89).

In addition to the check on our case A results discussed in Sec. IV we have performed a second and independent check by taking the $\lambda \to 0$ limit in the relevant exact expressions in Sec. IV. In this limit the exact result can be seen to factor into a Born term contribution times the soft-gluon factor given in Eq. (91). This proves that the exact results given in Sec. IV have the correct soft-gluon limiting behavior.

In order to be able to compare the eikonal SGA factor Eq. (89) and its approximate version Eq. (91) we (minimally) subtract the IR-divergent piece $h_{\rm IR}$ from both expressions where

$$h_{\rm IR} = -\frac{\alpha_s C_F}{\pi v}\left\{\left(2v + (2-\xi)\ln\left(\frac{1-v}{1+v}\right)\right)\ln\left(\frac{1}{\sqrt{\Lambda}}\right)\right\}. \quad (92)$$

The remaining IR finite pieces are then $h'_{\rm eik} = h_{\rm eik} - h_{\rm IR}$ and $h'_{\rm SGA} = h_{\rm SGA} - h_{\rm IR}$. In Fig. 3 we show a plot of the relative fraction $(h'_{\rm eik} - h'_{\rm SGA})/h'_{\rm SGA}$ as a function of the cutoff parameter $\lambda/\lambda_{\rm max}$. Figure 3 shows that $|h'_{\rm eik}| > |h'_{\rm SGA}|$ since both functions $h'_{\rm eik}$ and $h'_{\rm SGA}$ are negative over the whole range of λ. The SGA Eq. (91) is a poor approximation to the eikonal approximation Eq. (89) except for the region very close to the soft-gluon point. For $\sqrt{s} = 1000$ GeV the fractional deviation can become as large as 100% at the maximal cut value.

As it turns out the eikonal approximation with the eikonal factor (89) approximates the exact result rather well numerically even up to the hard end of the gluon spectrum. In Fig. 4 we show a plot of the total rate $\sigma(= \sigma_{U+L})$ as a function of the cutoff parameter $\lambda/\lambda_{\rm max}$ for the three center-of-mass energies $\sqrt{s} = 400$, 500, and 1000 GeV where we take $m_t = 175$ GeV and $\alpha_s = 0.0964$, 0.0941 and 0.0875, respectively, for the above three energies. The rates rise very quickly from the soft region to values close to the total rates showing that the contributions from the soft region dominate the total rates. The quality of the eikonal approximation becomes marginally weaker when the hard gluon region becomes larger with the increase of the center-of-mass energy. The exact result is hardly discernible from the eikonal result at the scale of the figure even for the highest c.m. energy. The SGA approximation can be seen to be quite poor. Also shown are the respective LO Born term contributions which appear as dotted horizontal lines in Fig. 4. The radiative corrections can be seen to be quite large. At the point where the $O(\alpha_s)$ rate intersects the LO Born term rate the α_s corrections go to zero. This can be seen to happen at $\lambda/\lambda_{\rm max} = 2 \times 10^{-6}$, 0.014,

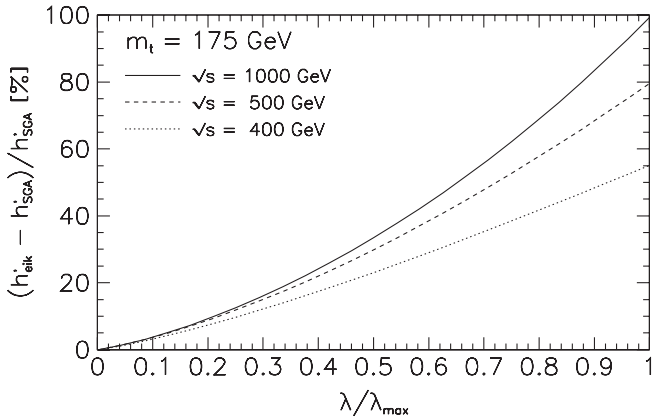

FIG. 3. Dependence of the relative fraction $(h'_{\rm eik} - h'_{\rm SGA})/h'_{\rm SGA}$ on the scaled gluon energy cutoff parameter $\lambda/\lambda_{\rm max}$ where $\lambda_{\rm max} = (1-\xi)/2$. Curves are shown for the three center-of-mass energies $\sqrt{s} = 400$ (dotted line), 500 (dashed line), and 1000 GeV (full line).

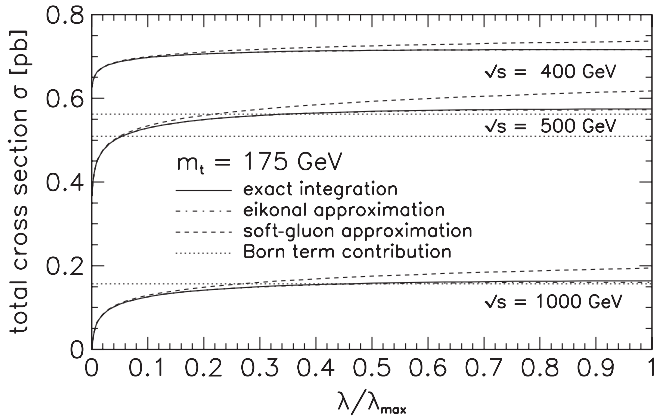

FIG. 4. Dependence of the total rate (solid line: exact NLO; dash-dotted line: eikonal; dashed line: SGA) on the scaled gluon energy cutoff parameter $\lambda/\lambda_{\max}$ where $\lambda_{\max} = (1-\xi)/2$. Also shown are the respective cutoff independent LO Born term contributions (horizontal dotted lines). Curves are shown for the three center-of-mass energies $\sqrt{s} = 400$, 500, and 1000 GeV.

and 0.200 for the above three c.m. energies. At even smaller cut values the total $O(\alpha_s)$ rate goes to zero altogether. This happens at $\lambda/\lambda_{\max} = 10^{-21}$, 10^{-8}, and 5×10^{-4} for the same three above c.m. energies. It is clear that perturbation theory should not be used for such small values of λ. This holds, in particular, for the polarization-type observables to be discussed later on since they are normalized to the total rate and are thus very sensitive to the vanishing of the total rate. It is important to keep in mind that the NLO rate goes to $-\infty$ when $\lambda \to 0$ even if this is not apparent in Fig. 4.

In order to show the quality of the eikonal approximation in Fig. 5 we show a plot of the cutoff dependence of the relative difference of the exact cross section and the eikonal approximation $(\sigma - \sigma_{\text{eik}})/\sigma$ for the same three center-of-mass energies. For $\sqrt{s} = 400$ GeV the relative difference is very small and remains below 0.1% over the

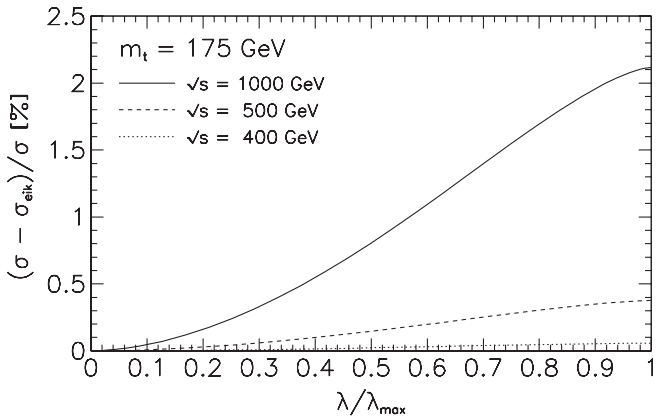

FIG. 5. Dependence of the relative difference of the exact cross section and the eikonal approximation on $\lambda/\lambda_{\max}$ where $\lambda_{\max} = (1-\xi)/2$ for center-of-mass energies $\sqrt{s} = 400$ (dotted line), 500 (dashed line), and 1000 GeV (full line).

whole gluon energy spectrum. For the largest energy shown ($\sqrt{s} = 1000$ GeV), where the hard gluon region is the largest, the relative difference rises from zero at the soft end of the spectrum to about 2% at the hard end of the spectrum.

VII. NUMERICAL RESULTS

Let us begin the numerical section by the statement that we shall, as in the previous section, always use a top quark mass of 175 GeV in our numerical results. Since all our results are given in analytical form the corresponding results for other values of the top quark mass can be readily calculated. For the strong coupling constant we take the same values as described at the end of the previous section.

We shall divide our numerical results into two sections according to whether the observables or structure functions have a nonvanishing or vanishing Born term contribution.

A. NLO corrections to nonvanishing LO observables

We shall use a terminology where the NLO results are partitioned into a soft and a hard region by a cutoff value for the gluon energy E_c. The soft and hard regions are defined by their respective integration regions. In the soft region one integrates from zero gluon energy up to the gluon energy cut E_c including, of course, the one-loop results. In the hard region, one integrates from the (lower) gluon energy cut E_c to the maximal gluon energy $E = (1-\xi)\sqrt{q^2}/2$. We use this terminology to differentiate between choosing an upper cutoff (soft region) and a lower cutoff (hard region) even if the respective integrations extend into regions with maximal and minimal gluon energy. The hard gluon contribution can be obtained by subtraction. Thus, for example, $\sigma(\text{hard}) = \sigma - \sigma(\text{soft})$. The definition of the two regions holds irrespective of the actual value of the cutoff energy.

In Fig. 6 we show a plot of the ratio $\sigma(\text{hard})/\sigma(\text{full})$ ($\sigma(\text{full}) = \sigma$) as a function of the cutoff parameter $\lambda/\lambda_{\max}$ for the three c.m. energies $\sqrt{s} = 400$, 500, and 1000 GeV. Note that the hard gluon fraction is proportional to α_s. The hard gluon fraction is generally quite small. As the lower cutoff tends to zero $\sigma(\text{hard})$ and thereby $\sigma(\text{hard})/\sigma(\text{full})$ tends to $+\infty$ (due to the positive $-\log\lambda$ singularity). Away from $\lambda = 0$ the hard gluon fraction then drops very quickly as the lower cutoff is raised and reaches zero at $\lambda/\lambda_{\max} = 1$ where there is no phase space left. The hard gluon fraction becomes larger as the energy increases. For example, at $\lambda/\lambda_{\max} = 0.2$ the hard gluon fraction is 1.5, 4.4, and 13.6% for $\sqrt{s} = 400$, 500, and 1000 GeV, respectively. The corresponding soft-gluon fractions can be obtained by subtraction as mentioned above.

We do not show corresponding plots for the other partial unpolarized and polarized rates $\sigma_i^{(m)}$ because they do not differ much from those shown in Fig. 6. This can be understood from the discussion in Sec. VI where we demon-

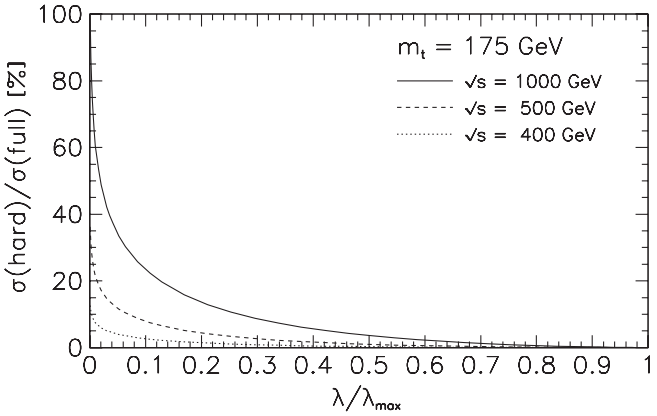

FIG. 6. Dependence of the ratio $\sigma(\text{hard})/\sigma(\text{full})$ on $\lambda/\lambda_{\max}$ in the hard region where λ denotes a lower cutoff. Curves are shown for the three center-of-mass energies $\sqrt{s} = 400$ (dotted line), 500 (dashed line), and 1000 GeV (full line).

strated that the real gluon emission contributions are very well approximated by the eikonal approximation which in turn is proportional to the Born term contribution. This implies that all ratios $\sigma_i^{(m)}(\text{hard})/\sigma_i^{(m)}(\text{full})$ are approximately equal to one another as well as approximately equal to $\sigma(\text{hard})/\sigma(\text{full})$. An exception is σ_L^{ℓ} where the Born term contribution is zero. This case will be discussed in more detail later on.

In Fig. 7 we show a plot of $d\sigma/d\cos\theta$ as a function of $\cos\theta$ for the three c.m. energies $\sqrt{s} = 400$, 500, and 1000 GeV and for three respective cutoff parameter values of $\lambda/\lambda_{\max} = 0.2$, 0.4, and 0.8. The $\cos\theta$ dependence is marked and strongest for $\sqrt{s} = 500$ GeV showing that the forward-backward contribution σ_F is non-neglible. The radiative corrections are large for $\sqrt{s} = 400$ GeV and $\sqrt{s} = 500$ GeV similar to the total rate plotted in Fig. 4. The cutoff dependence is generally quite weak showing that the bulk of the different partial rates comes from the region close to the soft-gluon point $\lambda = 0$.

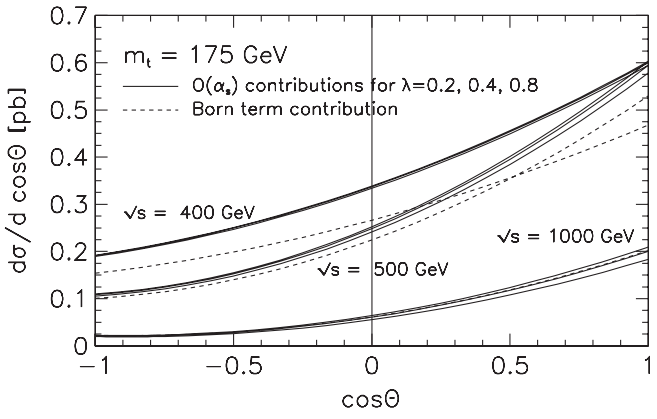

FIG. 7. Dependence of the differential rate $d\sigma/d\cos\theta$ on $\cos\theta$ in the soft region. Curves are shown for the three center-of-mass energies $\sqrt{s} = 400$ (dotted line), 500 (dashed line), and 1000 GeV (full line) and three upper cutoff values $\lambda/\lambda_{\max} = 0.2$, 0.4, and 0.8 (from bottom to top).

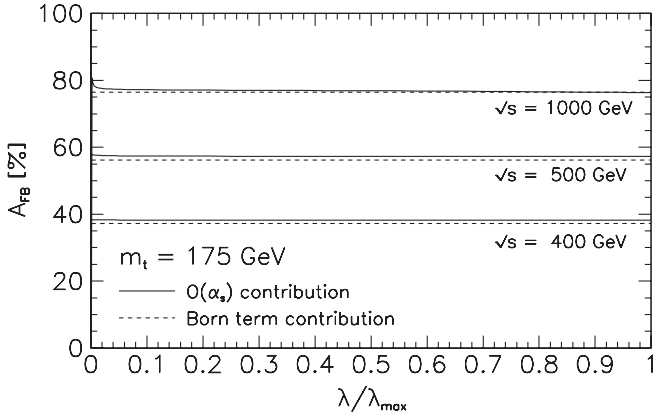

FIG. 8. Dependence of the forward-backward asymmetry A_{FB} on the (upper) cutoff $\lambda/\lambda_{\max}$ in the soft region (full line). Curves are shown for the three center-of-mass energies $\sqrt{s} = 400$, 500, and 1000 GeV. Also shown are the respective cutoff independent LO Born term contributions (horizontal dashed lines).

In Fig. 8 we show a plot of A_{FB} as a function of the upper cutoff $\lambda/\lambda_{\max}$ again for the three c.m. energies $\sqrt{s} = 400$, 500, and 1000 GeV where we have defined the forward-backward asymmetry by

$$A_{\text{FB}} = \frac{\sigma(\text{forward}) - \sigma(\text{backward})}{\sigma(\text{forward}) + \sigma(\text{backward})}. \tag{93}$$

Note that one has to separately integrate the numerator and denominator of Eq. (93) over the gluon energy when calculating A_{FB}. The radiative corrections are generally small and the dependence on the cutoff λ is quite weak. A_{FB} is largest for $\sqrt{s} = 1000$ GeV as can also be appreciated by looking at Fig. 7. The radiative corrections are largest for $\sqrt{s} = 400$ GeV. For example, for an upper cutoff of $\lambda/\lambda_{\max} = 0.2$ they amount to 2.7%.

The radiative corrections to polarization-type observables $P_i^{(m)}$ are in general quite small even if the radiative corrections to the polarized rates themselves are large. The reason is that polarization-type observables correspond to normalized density matrix elements defined by the ratio of a polarized rate and the total rate. The radiative corrections to the numerator and the denominator tend to go in the same direction and thus tend to cancel out in the ratio. Take, for example, a generic polarization observable $P_i^{(m)}$ which, at $O(\alpha_s)$, is defined by[3]

$$\begin{aligned} P_i^{(m)}(O(\alpha_s);\lambda) &= \frac{\sigma_i^{(m)}(\text{Born}) + \sigma_i^{(m)}(\alpha_s;\lambda)}{\sigma(\text{Born}) + \sigma(\alpha_s;\lambda)} \\ &\approx \frac{\sigma_i^{(m)}(\text{Born})(1 + h'_{\text{eik}}(\alpha_s;\lambda))}{\sigma(\text{Born})(1 + h'_{\text{eik}}(\alpha_s;\lambda))} \\ &= P_i^{(m)}(\text{Born}). \end{aligned} \tag{94}$$

[3]The forward-backward asymmetry A_{FB} defined in Eq. (93) is such a polarization-type observable with $\sigma_i^{(m)} = \sigma_F$.

Thus $P_i^{(m)}(O(\alpha_s);\lambda) = P_i^{(m)}(\text{Born})$ as long as one can neglect non-Born termlike structures in the radiative α_s corrections resulting either from the one-loop or the λ-dependent hard gluon corrections. As it turns out the non-Born termlike α_s corrections are in general small but can amount to several percent. The above reasoning breaks down when either the numerator or the denominator in Eq. (94) approaches zero which can happen for very small values of λ. As has been argued before such small cut values are not acceptable from the physics point of view.

In Fig. 9 we show a plot of P^ℓ as a function of $\lambda/\lambda_{\max}$ again for the three c.m. energies $\sqrt{s} = 400$, 500, and 1000 GeV where P^ℓ is the longitudinal polarization of the top quark $P^\ell = \sigma^\ell/\sigma$. Note that again one has to separately integrate the numerator and denominator over the gluon energy when calculating P^ℓ, i.e. $P^\ell(\lambda) = \sigma^\ell(\lambda)/\sigma(\lambda)$. As in Fig. 8 the radiative corrections and the dependence on λ can be seen to be quite small. The longitudinal polarization P^ℓ is largest for $\sqrt{s} = 1000$ GeV.

In order to highlight the size of the radiative corrections to P^ℓ we define a fractional deviation of P^ℓ from its Born term value for different cutoff values by writing

$$\delta(P^\ell) = \frac{P^\ell(\lambda) - P^\ell(\text{Born})}{P^\ell(\text{Born})}, \tag{95}$$

where $P^\ell(\lambda)$ is the value of P^ℓ for the upper cutoff parameter λ, i.e. in our above terminology $P^\ell(\lambda)$ refers to the value of the observable in the soft region. Figure 10 shows that close to $\lambda = 0$ the fractional deviations $\delta(P^\ell)$ tend to infinity because the denominator in $P^\ell(\lambda) = \sigma^\ell(\lambda)/\sigma(\lambda)$ goes to zero, as mentioned before. Away from $\lambda \approx 0$ the dependence of $\delta(P^\ell)$ on the gluon cut λ is not very pronounced except for the highest energy value $\sqrt{s} =$ 1000 GeV. The fractional deviation is largest for $\sqrt{s} =$ 400 GeV.

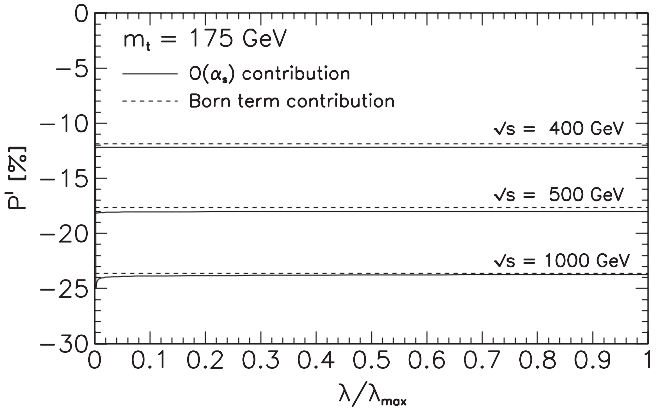

FIG. 9. Dependence of the longitudinal polarization P^ℓ on the (upper) cutoff $\lambda/\lambda_{\max}$ in the soft region (full line). Curves are shown for the three center-of-mass energies $\sqrt{s} = 400$, 500, and 1000 GeV. Also shown are the respective cutoff independent LO Born term contributions (horizontal dashed lines).

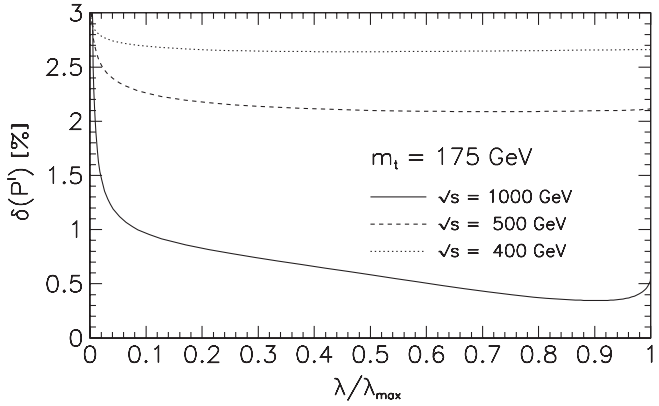

FIG. 10. Dependence of the fractional deviation of the longitudinal polarization $\delta(P^\ell)$ on the (upper) cutoff $\lambda/\lambda_{\max}$ in the soft region. Curves are shown for the three center-of-mass energies $\sqrt{s} = 400$ (dotted line), 500 (dashed line), and 1000 GeV (full line).

Also of interest are the values of a rate function in the hard gluon region. To this end we define a lower scaled gluon energy cutoff λ_{lower} and integrate from λ_{lower} to the upper limit $\lambda_{\max} = (1 - \xi)/2$. As before this is effectively done by subtraction, i.e. $\sigma^{(m)}(\text{hard}) = \sigma^{(m)}(\lambda_{\max}) - \sigma^{(m)}(\lambda)$ since we have not separately listed analytical formulas for the hard gluon rates. We then define a forward-backward asymmetry $A_{\text{FB}}(\text{hard})$ and a longitudinal polarization $P^\ell(\text{hard})$ in the hard region by writing

$$A_{\text{FB}}(\text{hard}) = \frac{\sigma(\text{forward}) - \sigma(\text{backward})}{\sigma(\text{forward}) + \sigma(\text{backward})}\Bigg|_{\text{hard}} \tag{96}$$

and

$$P^\ell(\text{hard}) = \frac{\sigma^\ell}{\sigma}\Bigg|_{\text{hard}}. \tag{97}$$

In Fig. 11 we show a plot of $A_{\text{FB}}(\text{hard})$ as a function of $\lambda/\lambda_{\max}$ again for the three c.m. energies $\sqrt{s} = 400$, 500, and 1000 GeV. As the lower cutoff tends to zero $A_{\text{FB}}(\text{hard})$ reaches values very close to those of $A_{\text{FB}}(\text{soft})$ in Fig. 8 showing that the non-Born term structures in the α_s-radiative corrections are not very significant. Only for larger cutoff values does one find significant deviation from the Born term values. For example, for $\lambda/\lambda_{\max} =$ 0.6 and $\sqrt{s} = 1000$ GeV one has a 30% deviation from the Born term value.

Figure 12 shows the same plot for the longitudinal polarization P^ℓ. Similar remarks apply as in the discussion of $A_{\text{FB}}(\text{hard})$ except that the dependence on the lower cutoff is not as pronounced as in Fig. 11. Marked deviations from the Born term values only set in at larger values of λ.

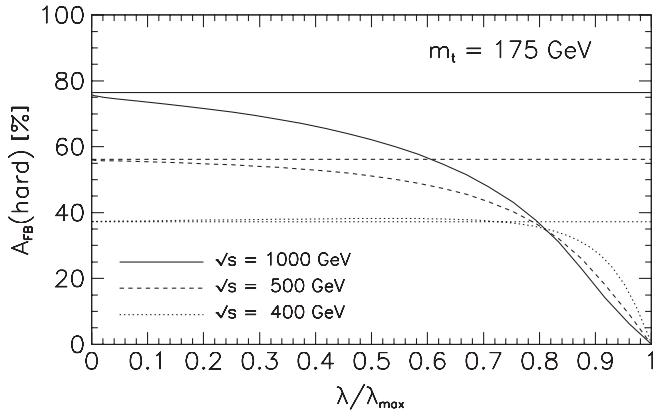

FIG. 11. Dependence of the forward-backward asymmetry A_{FB} on $\lambda/\lambda_{\max}$ in the hard region where λ denotes a lower cutoff. Curves are shown for the three center-of-mass energies $\sqrt{s} = 400$ (dotted line), 500 (dashed line), and 1000 GeV (full line). The straight lines indicate the Born term level results.

B. NLO contributions to vanishing LO observables or structure functions

It was pointed out already in Ref. [8] that the longitudinal polarization of the top quark produced from a longitudinally polarized gauge boson (γ and/or Z) denoted by P_L^ℓ vanishes at the Born term level. P_L^ℓ vanishes at the Born term level and also for the one-loop contribution due to the two facts that there are no second-class currents in the SM and that one is dealing with a two-body final state in these two cases. Technically this comes about since the contractions of the first class axial currents $\bar{u}\gamma_\mu\gamma_5 v$ and $\bar{u}q_\mu\gamma_5 v$ with the longitudinal projector e_3^μ [see Eq. (25)] vanish in the two-body case. In the standard model a nonvanishing value of the polarization P_L^ℓ is generated only at NLO (or higher orders) from real gluon bremsstrahlung. This NLO effect is quite small as can be seen from Fig. 2a in Ref. [8] which shows that P_L^ℓ rises from zero at threshold to -0.21% at $\sqrt{s} = 1000$ GeV.

A larger absolute value of P_L^ℓ is obtained in the hard gluon region since P_L^ℓ is an $O(\alpha_s)$ effect. To this end we define the ratio

$$P_L^\ell(\mathrm{hard}) = \frac{\sigma_L^\ell}{\sigma}\bigg|_{\mathrm{hard}}, \tag{98}$$

where the hard gluon region is defined as in the beginning of this section. In Fig. 13 we show a plot of $P_L^\ell(\mathrm{hard})$ as a function of the scaled gluon energy cutoff where the cutoff parameter λ now refers to a lower cutoff. It goes without saying that $P_L^\ell(\mathrm{hard}) = 0$ in the soft gluon or eikonal approximation since then $\sigma_L^\ell(\alpha_s) \propto \sigma_L^\ell(\mathrm{Born}) = 0$ in the soft gluon or eikonal approximation. Figure 13 shows that $P_L^\ell(\mathrm{hard})$ can become as large as -4% for $\sqrt{s} = 1000$ GeV and $\lambda/\lambda_{\max} = 0.8$. $P_L^\ell(\mathrm{hard})$ increases when the energy increases. $P_L^\ell(\mathrm{hard})$ goes to zero as $\lambda \to 0$ since in this limit σ_L^ℓ is finite whereas σ diverges.

We mention that a nonvanishing contribution to P_L^ℓ can also be obtained by adding an anomalous axial current to the usual SM first class top quark current structure. This will be discussed later on.

There are two classes of relations among the structure functions $H_a^{j(m)}$ at the two-body level. The first class of relations depends solely on the fact that one is dealing with a two-body final state at the Born term and one-loop level. There are four relations of this kind

$$\text{real part}: H_U^1 = H_F^{1\ell}, \qquad H_U^2 = H_F^{2\ell}, \qquad H_F^4 = H_U^{4\ell}, \tag{99}$$

$$\text{imaginary part}: H_F^3 = H_U^{3\ell}. \tag{100}$$

The second class of relations depends on the two-body dynamics and on the fact that one has only first class

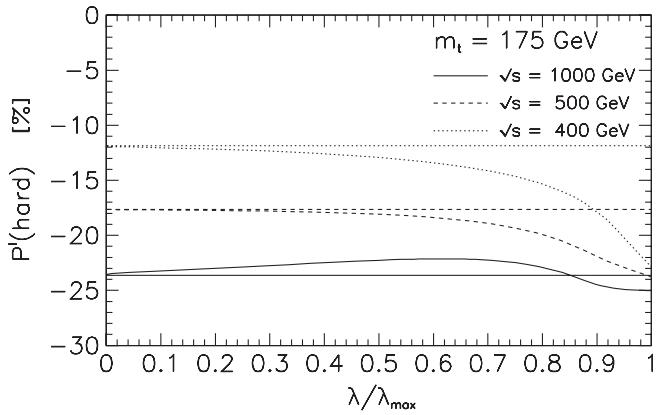

FIG. 12. Dependence of the longitudinal polarization P^ℓ on $\lambda/\lambda_{\max}$ in the hard region where λ denotes a lower cutoff. Curves are shown for the three center-of-mass energies $\sqrt{s} = 400$ (dotted line), 500 (dashed line), and 1000 GeV (full line). The straight lines indicate the Born term level results.

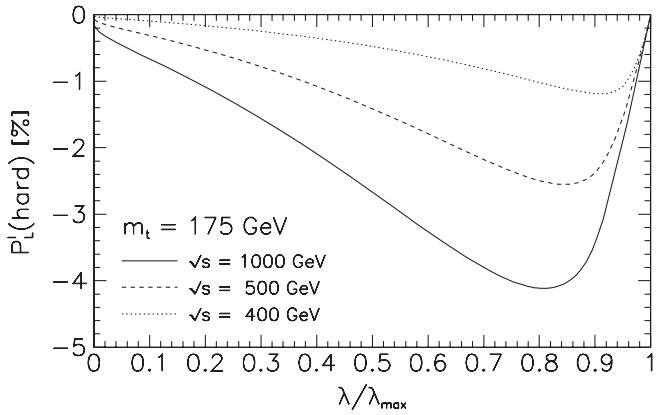

FIG. 13. Dependence of the longitudinal polarization from a longitudinal polarized gauge boson P_L^ℓ on $\lambda/\lambda_{\max}$ in the hard gluon region where λ denotes a lower cutoff. Curves are shown for the three center-of-mass energies $\sqrt{s} = 400$ (dotted line), 500 (dashed line), and 1000 GeV (full line).

currents in the SM. There are six relations of this kind. These are

$$\text{real part}: H_L^1 = H_L^2, \qquad H_L^{4\ell} = 0, \qquad H_A^{1T} = H_A^{2T}, \qquad H_A^{4T} = H_I^{3N}, \tag{101}$$

$$\text{imaginary part}: H_A^{4N} = H_I^{3T}, \qquad H_I^{1N} = H_I^{2N}. \tag{102}$$

One can explicitly check with the Born term and one-loop expressions listed in Sec. III that these relations are in fact satisfied.

Note that the class 1 relation $H_F^3 = H_U^{3\ell}$, and the class 2 relations $H_A^{4N} = H_I^{3T}$ and $H_I^{1N} = H_I^{2N}$ will not be affected by the $O(\alpha_s)$ tree graph contributions since they result from the imaginary parts of the (two-body) one-loop contributions. As mentioned before, the relation $H_U^2 = H_F^{2\ell}$ interestingly also holds at the $O(\alpha_s)$ tree graph level. In the following we shall numerically investigate how the remaining relations in (99) and (101) are affected by the $O(\alpha_s)$ tree graph contributions. It goes without saying that the relevant remaining relations in (99) and (101) still hold at NLO if one uses the soft-gluon or eikonal approximations rather than the exact form of the radiative corrections.

We start our numerical discussion with the first class of relations in Eq. (99). In order to obtain a quantitative handle on how the tree graph contributions affect the first class relations $H_U^1 = H_F^{1\ell}$ and $H_F^4 = H_U^{4\ell}$ in Eq. (99) we consider differences of the relevant structure functions and (arbitrarily) normalize them to $H_U^1(Born)$. In Fig. 14 we show a plot of the ratios $(H_U^1 - H_F^{1\ell})/H_U^1(\text{Born})$ and $(H_F^4 - H_U^{4\ell})/H_U^1(\text{Born})$ as functions of the upper cutoff ("soft region") in terms of the scaled gluon energy cut $\lambda/\lambda_{\max}$ for $\sqrt{s} = 500$ GeV. The violation of the class 1 relations slowly rises from zero at the soft-gluon point and reaches values of 0.27 and -0.02%, respectively, for the two above ratios at $\lambda_{\max}$ where one integrates over the full gluon phase space. In Fig. 15 we consider the hard region where $\lambda/\lambda_{\max}$ now refers to a lower cutoff in the gluon energy. Now $\lambda = 0$ corresponds to a full phase-space integration and one therefore recovers the $\lambda/\lambda_{\max} = 1$ limiting values of Fig. 14 remembering that there are no loop contributions to the above four quantities. The relevant ratios go to zero for $\lambda = \lambda_{\max}$ in Fig. 15 since phase space goes to zero.

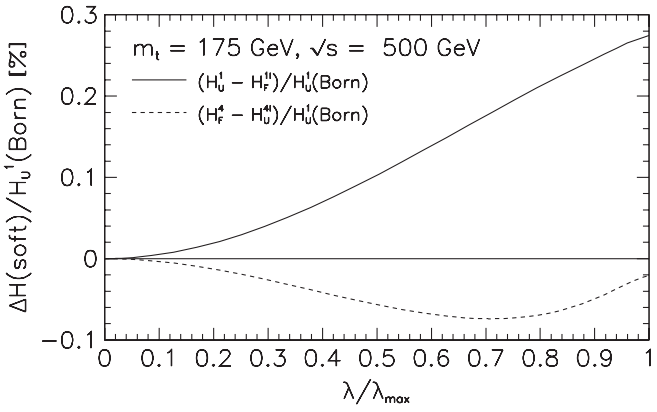

FIG. 14. Goodness of the class 1 relations against radiative corrections using an upper gluon energy cut. Dependence of the ratios $(H_U^1 - H_F^{1\ell})/H_U^1(\text{Born})$ (solid line), and $(H_F^4 - H_U^{4\ell})/H_U^1(\text{Born})$ (dashed line) on $\lambda/\lambda_{\max}$ where λ denotes an upper cutoff. Curves are shown for the center-of-mass energy $\sqrt{s} = 500$ GeV in the soft region.

The influence of the tree graph contributions on the second class of relations Eq. (101) is tested in a similar manner. We consider again differences of the relevant structure functions (or structure functions themselves) normalized to $H_U^1(\text{Born})$. In Figs. 16 and 17 we show plots of the ratios $(H_L^1 - H_L^2)/H_U^1(\text{Born})$, $H_L^{4\ell}/H_U^1(\text{Born})$, $(H_A^{1T} - H_A^{2T})/H_U^1(\text{Born})$, and $(H_I^{4T} - H_A^{3N})/H_U^1(\text{Born})$ for upper and lower cutoff values of the gluon energy, respectively. In Fig. 16 (soft region) the violations rise from zero at the soft-gluon point to the values 0.29, 0.15, 0.08, and 0.03% for $\lambda = \lambda_{\max}$ where one integrates over the full gluon phase space. Figure 17 shows the same four ratios in the hard gluon region. As before the rightmost values in Fig. 16 agree with their leftmost pendants in Fig. 17. The violations of the class 1 and class 2 relations due to hard gluon radiation can be seen to be generally quite small.

The effect of the radiative corrections to the class 2 relations (101) can be mimicked by adding an anomalous axial current to the SM currents. The anomalous axial current to be added reads (see e.g. [17,18])

$$j^\mu(\text{anomalous}) = g_a \bar{\psi}_t \frac{i\sigma^{\mu\nu} q_\nu}{2m_t} \gamma_5 \psi_t. \tag{103}$$

In general g_a can be complex, $g_a = \text{Re}g_a + i\,\text{Im}g_a$. Note that the current in Eq. (103) is a so-called second-class current with $J^{PC} = 1^{+-}$ quantum numbers. In particular, the contraction of the anomalous current with the longitudinal projector e_3^μ [see Eq. (25)] no longer vanishes, i.e. one now has $e_3^\mu \bar{u}\sigma_{\mu\nu}q^\nu v \neq 0$, and therefore $H_L^{4\ell} \neq 0$. It should be clear that the addition of the anomalous axial

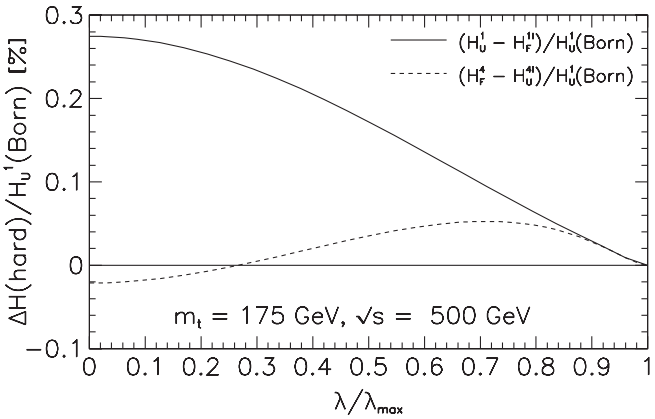

FIG. 15. The same as in Fig. 14 for the hard region.

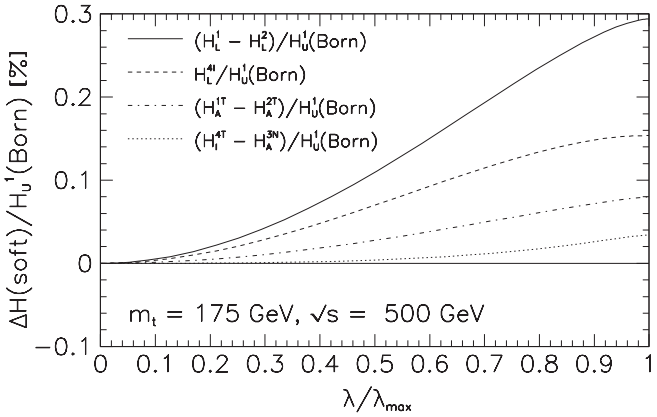

FIG. 16. Goodness of the class 2 relations against radiative corrections using an upper gluon energy cut. Dependence of the ratios $(H_L^1 - H_L^2)/H_U^1$(Born) (solid line), $H_L^{4\ell}/H_U^1$(Born) (dashed line), $(H_A^{1T} - H_A^{2T})/H_U^1$(Born) (dash-dotted line), and $(H_I^{4T} - H_A^{3N})/H_U^1$(Born) (dotted line) on $\lambda/\lambda_{\max}$ where λ denotes an upper cutoff. Curves are shown for the center-of-mass energy $\sqrt{s} = 500$ GeV.

current does not affect the class 1 two-body relations in Eq. (99) but, in general, violates the class 2 relations. We assume that the coupling strength g_a is small and we therefore only consider the interference contribution of Eq. (103) with the SM $(t\bar{t})$ current, i.e. terms that are linear in g_a.

The interference contribution of the anomalous axial-vector current can be calculated using the projection formulas written down in Sec. III. One finds

$$\begin{aligned} H_L^1 - H_L^2 &= O(g_a^2), \\ H_L^{4\ell} &= -2N_c q^2 v\, \mathrm{Re} g_a, \\ H_A^{1T} - H_A^{2T} &= N_c \frac{\sqrt{q^2}}{\sqrt{2}m} q^2 v^2\, \mathrm{Re} g_a, \\ H_I^{4T} - H_A^{3N} &= N_c \frac{\sqrt{q^2}}{\sqrt{2}m} q^2 v\, \mathrm{Re} g_a. \end{aligned} \tag{104}$$

It is noteworthy that only the real part of g_a contributes to the relations (104). In order to obtain a quantitative handle on the coupling parameter g_a we determine the values of the anomalous parameter g_a that would reproduce the fully integrated quantities $H_L^{4\ell}/H_U^1$(Born), $(H_A^{1T} - H_A^{2T})/H_U^1$(Born), and $(H_I^{4T} - H_A^{3N})/H_U^1$(Born), i.e. the values that these quantities take at the right-hand side of Fig. 16 at $\lambda/\lambda_{\max} = 1$. One finds $g_a = -0.0032$, 0.0023, and 0.0007 for $H_L^{4\ell}$, $H_A^{1T} - H_A^{2T}$, and $H_I^{4T} - H_A^{3N}$, respectively. Values substantially larger than these combinations of structure functions would signal contributions from a second-class current with coupling strength exceeding the above values of g_a.

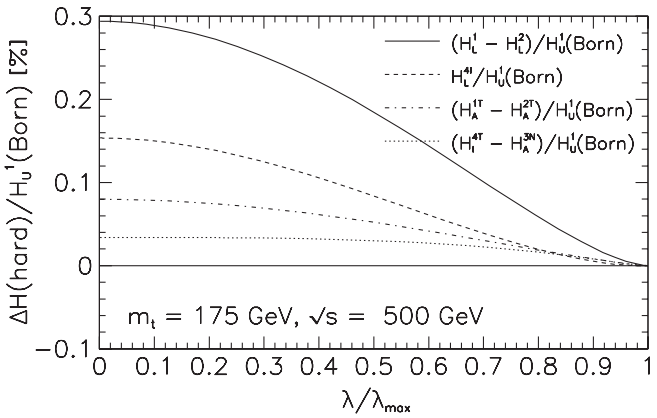

FIG. 17. The same as in Fig. 16 for the hard region.

VIII. SUMMARY AND OUTLOOK

We have presented analytical results for the $O(\alpha_s)$ radiative corrections to polarized top quark pair production in e^+e^- annihilation with a specific gluon energy cut. When the gluon energy cut is taken to its maximal value we recover previously known results [7,11]. The size of the radiative corrections to polarization-type observables involving the top quark is generally quite small in the soft-gluon region but can become substantial in the hard gluon region. This in turn implies that the dependence of the polarization-type observables on the gluon energy cut is generally quite small in the soft-gluon region but can become large in the hard gluon region. We have calculated the contributions of a CP-odd non-SM coupling to some linear combinations of structure functions that vanish in the two-body SM case. These were compared to SM contributions resulting from radiative corrections.

We have not considered beam polarization effects in our analysis. However, in as much as we have calculated the complete set of single spin structure functions, beam polarization effects can be easily incorporated into our analysis as described e.g. in more detail in Ref. [8].

We have decomposed the top spin vector in the helicity basis, i.e. the z direction of our spin basis is determined by the momentum of the top quark. In addition to the helicity basis the authors of Refs. [16,19] have also considered a beam line and an off-diagonal basis. A discussion of how these bases are related to the helicity basis in the context of the NLO corrections can be found in Ref. [11].

All the results in this paper refer to the polarization of the top quark. In order to obtain the SM and anomalous coupling predictions for the polarization of the antitop quark let us first set up an orthonormal spin basis for the antitop quark by replacing the momenta in Eq. (4) by their charge conjugate partners, i.e. $\vec{p}_1 \to \vec{p}_2$ and $\vec{p}_{e^-} \to \vec{p}_{e^+}$. The three orthonormal basis vectors $(\vec{e}_T, \vec{e}_N, \vec{e}_\ell)$ are now given by

$$\vec{e}_T = \frac{(\vec{p}_{e^+} \times \vec{p}_2) \times \vec{p}_2}{|(\vec{p}_{e^+} \times \vec{p}_2) \times \vec{p}_2|}, \qquad \vec{e}_N = \frac{\vec{p}_{e^+} \times \vec{p}_2}{|\vec{p}_{e^+} \times \vec{p}_2|}, \qquad \vec{e}_\ell = \frac{\vec{p}_2}{|\vec{p}_2|}. \tag{105}$$

In the polar angle distribution Eq. (8) the polar angle now

refers to $\theta_{\bar{t}e^-}$ and *not* to $\theta = \theta_{te^-}$ as in the top quark case discussed in the main part of this paper. Since the lepton pair is back to back, one has $\theta_{\bar{t}e^-} = \pi - \theta_{\bar{t}e^+}$, i.e. the two terms in Eq. (8) proportional to $\cos\theta$ change sign if written in terms of $\cos\theta_{\bar{t}e^+}$.

Let us list the SM Born term and the anomalous contributions in the antitop quark case given by Eq. (103) together with the relevant contributions in the top quark case. One finds

$$
\begin{aligned}
&H_U^1 = 2N_C q^2(1+v^2), \quad H_U^2 = 2N_C q^2(1-v^2), \quad H_U^{3\ell} = 0, \quad H_U^{4\ell} = \pm 4N_C q^2 v,\\
&H_L^1 = N_C q^2(1-v^2) + N_C q^2 v^2 \frac{|g_a|^2}{\xi}, \quad H_L^2 = N_C q^2(1-v^2) - N_C q^2 v^2 \frac{|g_a|^2}{\xi}, \quad H_L^{3\ell} = -2N_C q^2 v\,\mathrm{Im} g_a,\\
&H_L^{4\ell} = -2N_C q^2 v\,\mathrm{Re} g_a, \quad H_F^{1\ell} = 2N_C q^2(1+v^2), \quad H_F^{2\ell} = 2N_C q^2(1-v^2), \quad H_F^3 = 0, \quad H_F^4 = \pm 4N_c q^2 v,\\
&H_I^{3T} = \frac{N_C q^2}{\sqrt{2\xi}} v\,\mathrm{Im} g_a, \quad H_I^{4T} = \frac{N_C q^2}{\sqrt{2\xi}} v(\pm\xi + \mathrm{Re} g_a), \quad H_A^{1T} = \frac{N_C q^2}{\sqrt{2\xi}}(\xi \pm v^2\,\mathrm{Re} g_a), \quad H_A^{2T} = \frac{N_C q^2}{\sqrt{2\xi}}(\xi \mp v^2\,\mathrm{Re} g_a),\\
&H_I^{1N} = \pm\frac{N_C q^2}{\sqrt{2\xi}} v^2\,\mathrm{Im} g_a, \quad H_I^{2N} = \mp\frac{N_C q^2}{\sqrt{2\xi}} v^2\,\mathrm{Im} g_a, \quad H_A^{3N} = \frac{N_C q^2}{\sqrt{2\xi}} v(\pm\xi - \mathrm{Re} g_a), \quad H_A^{4N} = \frac{N_C q^2}{\sqrt{2\xi}} v\,\mathrm{Im} g_a, \qquad (106)
\end{aligned}
$$

where the upper and lower signs refer to the top quark and antitop quark cases, respectively. As concerns the SM Born term contributions one finds

$$
\begin{aligned}
\sigma_t(\cos\theta_{te^-}) &= \sigma_{\bar{t}}(\cos\theta_{\bar{t}e^+}),\\
P_t^{\ell,N}(\cos\theta_{te^-}) &= -P_{\bar{t}}^{\ell,N}(\cos\theta_{\bar{t}e^+}), \qquad (107)\\
P_t^T(\cos\theta_{te^-}) &= P_{\bar{t}}^T(\cos\theta_{\bar{t}e^+}).
\end{aligned}
$$

In the three-body case one has to simultaneously exchange $(y \leftrightarrow z)$ in the SM part of Eqs. (106) and (107). For example, one has $H_L^{3,4\ell}(\mathrm{top}; y, z) = -H_L^{3,4\ell}(\mathrm{antitop}; z, y)$. If one performs an integration symmetric in y and z as done in this paper the SM part of the relations (106) and (107) also hold for the integrated three-body results.

The linear contributions of the anomalous coupling to the polarization vector behave in the opposite way to those in Eq. (107), i.e.

$$
\begin{aligned}
P_t^{\ell,N}(\mathrm{anomalous}; \cos\theta_{te^-}) &= P_{\bar{t}}^{\ell,N}(\mathrm{anomalous}; \cos\theta_{\bar{t}e^+}),\\
P_t^T(\mathrm{anomalous}; \cos\theta_{te^-}) &= -P_{\bar{t}}^T(\mathrm{anomalous}; \cos\theta_{\bar{t}e^+}). \qquad (108)
\end{aligned}
$$

It is clear that one can obtain an additional handle on the anomalous contributions by taking sums and differences of the top quark and antitop quark polarizations. For example, $[P_t^{\ell,N}(\cos\theta_{te^-}) + P_{\bar{t}}^{\ell,N}(\cos\theta_{\bar{t}e^+})]$ and $[P_t^T(\cos\theta_{te^-}) - P_{\bar{t}}^T(\cos\theta_{\bar{t}e^+})]$ are contributed to only by the anomalous contributions.

In this paper we have not discussed how the spin of the top quark can be analyzed. The top quark decays weakly and is therefore self-analyzing. If one assumes SM interactions in the cascade decay $t \to bW^+(\to l^+\nu_l, q\bar{q})$ the polarization of the top quark can be reconstructed by measuring spin-momentum correlations either in the top quark rest system (see e.g. Refs. [20–23]) or in the W rest system as e.g. discussed in Refs. [15,24,25]. We mention that there exists a large body of literature of how non-SM interactions in the production (see e.g. Ref. [26]) [such as the anomalous coupling Eq. (103)], and/or in the decay affect such spin-momentum correlations (see e.g. Ref. [27] and references therein).

Gluons can be emitted from the original production process $e^+e^- \to t\bar{t}(G)$ as well as from the follow-up decay process $t \to b + W^+(G)$ and $\bar{t} \to \bar{b} + W^-(G)$ where we take the W's to decay leptonically. Interference effects between the two processes are expected to be quite small since they are suppressed by a factor of $\approx \Gamma_t/m_t \sim 1\%$. In order to identify the gluons of the original production process (which are the subject of this paper) one has to demand that the gluon's four-momentum satisfies $q = p_t + p_{\bar{t}} + p_G$. Gluons that satisfy $p_t = p_b + p_W + p_G$ or $p_{\bar{t}} = p_{\bar{b}} + p_W + p_G$ clearly originate from the follow-up processes and can thus be vetoed. How effectively gluons not originating from the original production process can be removed from the data sample has to be carefully studied in detailed Monte Carlo simulation runs.

With the appropriate modifications our results can also be applied to the $(b\bar{b})$ case. While the $\mathrm{Im}\chi_Z$ contributions resulting from the imaginary part of the Breit-Wigner line shape are negligibly small in the $(t\bar{t})$ case [since $(t\bar{t})$ threshold is far away from the Z pole] the $\mathrm{Im}\chi_Z$ contribution is more pronounced in the $(b\bar{b})$ case, in particular, in the vicinity of the Z pole. However, close to the Z pole the transverse and normal polarizations of the bottom quark are severely suppressed due to the overall helicity suppression factor $2m/\sqrt{s}$. In this sense the phenomenology of the top quark spin above $(t\bar{t})$ threshold is richer than that of the bottom quark in the high energy realm.

ACKNOWLEDGMENTS

We would like to thank V. Kleinschmidt for participating in the early stages of this calculation. We are also grateful for illuminating discussions with G. J. Gounaris and F. M. Renard. This work is supported in part by the Estonian

target financed project No. 0182647s04 and by the Estonian Science Foundation under Grant No. 6216. S. G. also acknowledges support from a grant of the Deutsche Forschungsgemeinschaft (DFG) for staying at Mainz University as a guest scientist for a couple of months.

APPENDIX A: SM VALUES OF THE ELECTROWEAK COUPLING COEFFICIENTS

The electroweak coupling matrix elements $g_{ij}(q^2)$ are given by

$$\begin{aligned}
&g_{11} = Q_f^2 - 2Q_f v_e v_f \,\mathrm{Re}\chi_Z + (v_e^2 + a_e^2)(v_f^2 + a_f^2)|\chi_Z|^2,\\
&g_{12} = Q_f^2 - 2Q_f v_e v_f \,\mathrm{Re}\chi_Z + (v_e^2 + a_e^2)(v_f^2 - a_f^2)|\chi_Z|^2, \qquad g_{13} = -2Q_f v_e a_f \,\mathrm{Im}\chi_Z,\\
&g_{14} = 2Q_f v_e a_f \,\mathrm{Re}\chi_Z - 2(v_e^2 + a_e^2) v_f a_f |\chi_Z|^2, \; g_{21} = Q_f^2 - 2Q_f v_e v_f \,\mathrm{Re}\chi_Z + (v_e^2 - a_e^2)(v_f^2 + a_f^2)|\chi_Z|^2,\\
&g_{22} = Q_f^2 - 2Q_f v_e v_f \,\mathrm{Re}\chi_Z + (v_e^2 - a_e^2)(v_f^2 - a_f^2)|\chi_Z|^2, \qquad g_{23} = -2Q_f v_e a_f \,\mathrm{Im}\chi_Z,\\
&g_{24} = 2Q_f v_e a_f \,\mathrm{Re}\chi_Z - 2(v_e^2 - a_e^2) v_f a_f |\chi_Z|^2, \; g_{31} = -2Q_f a_e v_f \,\mathrm{Im}\chi_Z, \qquad g_{32} = -2Q_f a_e v_f \,\mathrm{Im}\chi_Z,\\
&g_{33} = 2Q_f a_e a_f \,\mathrm{Re}\chi_Z, \qquad g_{34} = 2Q_f a_e a_f \,\mathrm{Im}\chi_Z, \; g_{41} = 2Q_f a_e v_f \,\mathrm{Re}\chi_Z - 2v_e a_e (v_f^2 + a_f^2)|\chi_Z|^2,\\
&g_{42} = 2Q_f a_e v_f \,\mathrm{Re}\chi_Z - 2v_e a_e (v_f^2 - a_f^2)|\chi_Z|^2, \qquad g_{43} = 2Q_f a_e a_f \,\mathrm{Im}\chi_Z,\\
&g_{44} = -2Q_f a_e a_f \,\mathrm{Re}\chi_Z + 4v_e a_e v_f a_f |\chi_Z|^2,
\end{aligned} \tag{A1}$$

where $\chi_Z(q^2) = gM_Z^2 q^2/(q^2 - M_Z^2 + iM_Z\Gamma_Z)$, with M_Z and Γ_Z the mass and width of the Z^0 and $g = G_F(8\sqrt{2}\pi\alpha)^{-1} \approx 4.49 \times 10^{-5}\ \mathrm{GeV}^{-2}$. Q_f are the charges of the final state quarks to which the electroweak currents directly couple; v_e and a_e, v_f and a_f are the electroweak vector and axial-vector coupling constants. For example, in the Weinberg-Salam model, one has $v_e = -1 + 4\sin^2\theta_W$, $a_e = -1$ for leptons, $v_f = 1 - \frac{8}{3}\sin^2\theta_W$, $a_f = 1$ for up-type quarks ($Q_f = \frac{2}{3}$), and $v_f = -1 + \frac{4}{3}\sin^2\theta_W$, $a_f = -1$ for down-type quarks ($Q_f = -\frac{1}{3}$). The left- and right-handed coupling constants are then given by $g_L = v + a$ and $g_R = v - a$, respectively. In the purely electromagnetic case one has $g_{11} = g_{12} = g_{21} = g_{22} = Q_f^2$ and all other $g_{r's} = 0$. The terms linear in $\mathrm{Re}\chi_Z$ and $\mathrm{Im}\chi_Z$ come from $\gamma - Z^0$ interference, whereas the terms proportional to $|\chi_Z|^2$ originate from Z exchange.

Contributions coming from the imaginary part of the Breit-Wigner resonance shape are of order $O(\mathrm{Im}\chi_Z(q^2)/\mathrm{Re}\chi_Z(q^2))$ and can thus safely be neglected for top quark pair production. For example, in the threshold region of top quark pair production $\mathrm{Im}\chi_Z/\mathrm{Re}\chi_Z$ is approximately 0.1% and decreases further with a $1/q^2$ power falloff behavior.

APPENDIX B: DECAY RATE TERMS t_i

It is convenient to define the mass dependent variables $a := 2 + \sqrt{\xi}$, $b := 2 - \sqrt{\xi}$, and $w := \sqrt{(1-\sqrt{\xi})/(1+\sqrt{\xi})}$. The rate functions $t_1, \ldots, t_{12}$ appearing in the main text are then given by

$$\begin{aligned}
t_1 &:= \ln\left(\frac{2\xi\sqrt{\xi}}{b^2(1+\sqrt{\xi})}\right),\\
t_2 &:= \ln\left(\frac{2\sqrt{\xi}}{1+\sqrt{\xi}}\right) \Rightarrow t_1 - t_2 = \ln\left(\frac{\xi}{b^2}\right),
\end{aligned} \tag{B1}$$

$$t_3 := \ln\left(\frac{1+v}{1-v}\right), \tag{B2}$$

$$t_4 := \mathrm{Li}_2(w) - \mathrm{Li}_2(-w) + \mathrm{Li}_2\left(\frac{a}{b}w\right) - \mathrm{Li}_2\left(-\frac{a}{b}w\right), \tag{B3}$$

$$\begin{aligned}
t_5 := {}& \frac{1}{2}\ln\left(\frac{a\sqrt{\xi}}{4(1+\sqrt{\xi})}\right)\ln\left(\frac{1+v}{1-v}\right) + \mathrm{Li}_2\left(\frac{2\sqrt{\xi}}{a(1+w)}\right)\\
&- \mathrm{Li}_2\left(\frac{2\sqrt{\xi}}{a(1-w)}\right) + \mathrm{Li}_2\left(\frac{1+w}{2}\right) - \mathrm{Li}_2\left(\frac{1-w}{2}\right)\\
&+ \mathrm{Li}_2\left(\frac{a(1+w)}{4}\right) - \mathrm{Li}_2\left(\frac{a(1-w)}{4}\right),
\end{aligned} \tag{B4}$$

$$\begin{aligned}
t_6 := {}& \ln^2(1+w) + \ln^2(1-w) + \ln\left(\frac{a}{8}\right)\ln(1-w^2)\\
&+ \mathrm{Li}_2\left(\frac{2\sqrt{\xi}}{a(1+w)}\right) + \mathrm{Li}_2\left(\frac{2\sqrt{\xi}}{a(1-w)}\right) - 2\mathrm{Li}_2\left(\frac{2\sqrt{\xi}}{a}\right)\\
&+ \mathrm{Li}_2\left(\frac{1+w}{2}\right) + \mathrm{Li}_2\left(\frac{1-w}{2}\right) - 2\mathrm{Li}_2\left(\frac{1}{2}\right)\\
&+ \mathrm{Li}_2\left(\frac{a(1+w)}{4}\right) + \mathrm{Li}_2\left(\frac{a(1-w)}{4}\right) - 2\mathrm{Li}_2\left(\frac{a}{4}\right),
\end{aligned} \tag{B5}$$

$$t_7 := 2\ln\left(\frac{1-\xi}{2\xi}\right)\ln\left(\frac{1+v}{1-v}\right) - \mathrm{Li}_2\left(\frac{2v}{(1+v)^2}\right) + \mathrm{Li}_2\left(-\frac{2v}{(1-v)^2}\right) - \frac{1}{2}\mathrm{Li}_2\left(-\left(\frac{1+v}{1-v}\right)^2\right) + \frac{1}{2}\mathrm{Li}_2\left(-\left(\frac{1-v}{1+v}\right)^2\right) + \mathrm{Li}_2\left(\frac{2w}{1+w}\right) - \mathrm{Li}_2\left(-\frac{2w}{1-w}\right) - 2\mathrm{Li}_2\left(\frac{w}{1+w}\right) + 2\mathrm{Li}_2\left(-\frac{w}{1-w}\right) + \mathrm{Li}_2\left(\frac{2aw}{b+aw}\right) - \mathrm{Li}_2\left(-\frac{2aw}{b-aw}\right) - 2\mathrm{Li}_2\left(\frac{aw}{b+aw}\right) + 2\mathrm{Li}_2\left(-\frac{aw}{b-aw}\right), \tag{B6}$$

$$t_8 := \ln\left(\frac{\xi}{4}\right)\ln\left(\frac{1+v}{1-v}\right) + \mathrm{Li}_2\left(\frac{2v}{1+v}\right) - \mathrm{Li}_2\left(-\frac{2v}{1-v}\right) - \pi^2, \tag{B7}$$

$$t_9 := 2\ln\left(\frac{2(1-\xi)}{\sqrt{\xi}}\right)\ln\left(\frac{1+v}{1-v}\right) + 2\left(\mathrm{Li}_2\left(\frac{1+v}{2}\right) - \mathrm{Li}_2\left(\frac{1-v}{2}\right)\right) + 3\left(\mathrm{Li}_2\left(-\frac{2v}{1-v}\right) - \mathrm{Li}_2\left(\frac{2v}{1+v}\right)\right), \tag{B8}$$

$$t_{10} := \ln\left(\frac{4}{\xi}\right), \qquad t_{11} := \ln\left(\frac{4(1-\sqrt{\xi})^2}{\xi}\right), \qquad t_{12} := \ln\left(\frac{4(1-\xi)}{\xi}\right). \tag{B9}$$

APPENDIX C: DECAY RATE TERMS ℓ_i, $t_{0\pm}$, $t_{1\pm}$, AND t_w

The logarithmic rate terms ℓ_i are given by

$$\ell_1 = \ln\left(\frac{w_1^2 - w_\lambda^2}{w_0^2 - w_1^2}\right) - \ln\left(\frac{1+w_1}{b-aw_1}\right) - \ln\left(\frac{(1+\sqrt{\xi})\sqrt{\xi}}{1-2\lambda+\sqrt{\xi}}\right), \tag{C1}$$

$$\ell_2 = \ln\left(\frac{w_2^2 - w_\lambda^2}{w_0^2 - w_2^2}\right) + \ln\left(\frac{b+aw_2}{1-w_2}\right) - \ln\left(\frac{(1+\sqrt{\xi})\sqrt{\xi}}{1-2\lambda+\sqrt{\xi}}\right), \tag{C2}$$

$$\ell_3 = \ln\left(\frac{w_2}{w_1}\right), \tag{C3}$$

$$\ell_{4+} = -\frac{\lambda\xi}{y_1} + \frac{\lambda\xi}{y_2} + 2v\left[4 - 2\ln\left(\frac{4w_0y_1}{\sqrt{\xi}}\right) + \ln\left(\frac{w_0+w_1}{w_0-w_1}\right) + \ln\left(\frac{w_0+w_2}{w_0-w_2}\right)\right] + \left(2v - (2-\xi)\ln\left(\frac{1+v}{1-v}\right)\right) \times \left[\ln\left(\frac{\xi\Lambda}{v^2}\right) + 2\ln\left(\frac{w_0^2-w_1^2}{1-w_1^2}\right) - 1\right], \tag{C4}$$

$$\ell_{4-} = 2v\left[2 - 2\ln\left(\frac{2\sqrt{\xi}y_1}{v}\right) + \ln\left(\frac{(1+w_1)(b-aw_1)}{w_0^2-w_1^2}\right) + \ln\left(\frac{(b+aw_2)(1-w_2)}{w_0^2-w_2^2}\right)\right] + \left(2v - (2-\xi) \times \ln\left(\frac{1+v}{1-v}\right)\right)\left[\ln\left(\frac{\xi\Lambda}{v^2}\right) + 2\ln\left(\frac{w_0^2-w_1^2}{1-w_1^2}\right) - 1\right], \tag{C5}$$

$$\ell_{5+} = \ln\left(\frac{1-w_2}{1-w_0}\right) - \ln\left(\frac{1+w_1}{1+w_0}\right), \qquad \ell_{5-} = 2\ln\left(\frac{1+v}{1-v}\right), \tag{C6}$$

$$\ell_{6+} = 2\ln\left(\frac{1+v}{1-v}\right) - \ln\left(\frac{1+w_1}{b-aw_1}\right) - \ln\left(\frac{b+aw_2}{1-w_2}\right), \tag{C7}$$

$$\ell_{6-} = \ln\xi + \ln\left(\frac{1+w_1}{b-aw_1}\right) - \ln\left(\frac{b+aw_2}{1-w_2}\right), \tag{C8}$$

$$\ell_{7+} = \ln\left(\frac{w_2^2 - w_\lambda^2}{w_1^2 - w_\lambda^2}\right), \qquad \ell_{7-} = \ln\left(\frac{w_2 - w_\lambda}{w_1 - w_\lambda}\right) - \ln\left(\frac{w_2 + w_\lambda}{w_1 + w_\lambda}\right), \tag{C9}$$

$$\ell_{8+} = \ln\left(\frac{w_0^2 - w_2^2}{w_0^2 - w_1^2}\right), \qquad \ell_{8-} = \ln\left(\frac{w_0 - w_2}{w_0 - w_1}\right) - \ln\left(\frac{w_0 + w_2}{w_0 + w_1}\right), \tag{C10}$$

$$\ell_{9+} = \ln\left(\frac{1-w_2^2}{1-w_1^2}\right), \qquad \ell_{9-} = \ln\left(\frac{1-w_2}{1-w_1}\right) - \ln\left(\frac{1+w_2}{1+w_1}\right), \tag{C11}$$

while for the additional phase-space contribution we have to use

$$\ell_2^c = \ln\left(\frac{1+w_2}{1-w_2}\right) + \ln\left(\frac{b+aw_2}{b-aw_2}\right), \qquad \ell_{4-}^c = \ln(1-w_2^2) + \ln(b^2-a^2w_2^2), \qquad \ell_{4+}^c = \ln\left(\frac{w_0+w_2}{w_0-w_2}\right),$$
$$\ell_{5-}^c = \ln b = \ln(2-\sqrt{\xi}), \qquad \ell_{5+}^c = \ln\left(\frac{1+w_2}{1-w_2}\right), \qquad \ell_{6-}^c = \ln(1-w_2^2) - \ln(b^2-a^2w_2^2), \qquad \ell_{7-}^c = \ln\left(\frac{w_0^2}{w_0^2-w_2^2}\right). \tag{C12}$$

For the double and dilogarithmic decay rate terms we obtain

$$t_w = \frac{1}{2}(2t_w^{ba}(w_0) - t_w^{ba}(w_1) - t_w^{ba}(w_2)) + (t_w^z(w_2) - t_w^z(w_1)) - \frac{1}{2}(t_w^{ab}(w_2) - t_w^{ab}(w_1)) - (t_w^\lambda(w_2) - t_w^\lambda(w_1)) + \ln\left(\frac{(1+\sqrt{\xi})\sqrt{\xi}}{1-2\lambda+\sqrt{\xi}}\right)\ln\left(\frac{w_2}{w_1}\right), \tag{C13}$$

$$t_{0\pm} = \frac{1}{2}(2t_{0\pm}^{ba}(w_0) - t_{0\pm}^{ba}(w_1) - t_{0\pm}^{ba}(w_2)) + (t_{0\pm}^z(w_2) - t_{0\pm}^z(w_1)) - \frac{1}{2}(t_{0\pm}^{ab}(w_2) - t_{0\pm}^{ab}(w_1)) - (t_{0\pm}^\lambda(w_2) - t_{0\pm}^\lambda(w_1)) \pm \ln\left(\frac{(1+\sqrt{\xi})\sqrt{\xi}}{1-2\lambda+\sqrt{\xi}}\right)\ln\left(\frac{w_0 \pm w_2}{w_0 \pm w_1}\right), \tag{C14}$$

$$t_{1\pm} = \frac{1}{2}(2t_{1\pm}^{ba}(w_0) - t_{1\pm}^{ba}(w_1) - t_{1\pm}^{ba}(w_2)) + (t_{1\pm}^z(w_2) - t_{1\pm}^z(w_1)) - \frac{1}{2}(t_{1\pm}^{ab}(w_2) - t_{1\pm}^{ab}(w_1)) - (t_{1\pm}^\lambda(w_2) - t_{1\pm}^\lambda(w_1)) \pm \ln\left(\frac{(1+\sqrt{\xi})\sqrt{\xi}}{1-2\lambda+\sqrt{\xi}}\right)\ln\left(\frac{1 \pm w_2}{1 \pm w_1}\right), \tag{C15}$$

while for the additional phase-space contribution we take

$$t_w^c = t_w^{ba}(w_2) - t_w^{ba}(0), \qquad t_{0\pm}^c = t_{0\pm}^{ba}(w_2) - t_{0\pm}^{ba}(0), \qquad t_{1\pm}^c = t_{1\pm}^{ba}(w_2) - t_{1\pm}^{ba}(0), \tag{C16}$$

where

$$\begin{aligned} t_w^{ba}(w) &= \mathrm{Li}_2(w) - \mathrm{Li}_2(-w) + \mathrm{Li}_2\left(\frac{aw}{b}\right) - \mathrm{Li}_2\left(\frac{-aw}{b}\right), \\ t_w^z(w) &= 2\ln(w_0)\ln(w) + \mathrm{Li}_2(w) - \mathrm{Li}_2(-w) - \mathrm{Li}_2\left(\frac{w}{w_0}\right) - \mathrm{Li}_2\left(\frac{-w}{w_0}\right), \\ t_w^{ab}(w) &= 2\ln(b)\ln(w) + \mathrm{Li}_2(w) - \mathrm{Li}_2(-w) - \mathrm{Li}_2\left(\frac{aw}{b}\right) - \mathrm{Li}_2\left(\frac{-aw}{b}\right), \\ t_w^\lambda(w) &= \ln^2(w) + \mathrm{Li}_2(w) + \mathrm{Li}_2(-w) + \mathrm{Li}_2\left(\frac{w_\lambda}{w}\right) + \mathrm{Li}_2\left(\frac{-w_\lambda}{w}\right), \end{aligned} \tag{C17}$$

$$t_{0-}^{ba}(w) = -2\ln\left(\frac{1+v}{1-v}\right)\ln(w_0-w) + \mathrm{Li}_2\left(\frac{w_0-w}{w_0+1}\right) - \mathrm{Li}_2\left(\frac{w_0-w}{w_0-1}\right) + \mathrm{Li}_2\left(\frac{a(w_0-w)}{aw_0+b}\right) - \mathrm{Li}_2\left(\frac{a(w_0-w)}{aw_0-b}\right),$$

$$t_{0-}^{ba}(w_0) = 2\ln\left(\frac{y_1}{\sqrt{\xi}}\right)\ln\left(\frac{1+v}{1-v}\right) - \mathrm{Li}_2\left(\frac{2v}{(1+v)^2}\right) + \mathrm{Li}_2\left(\frac{-2v}{(1-v)^2}\right) + \frac{1}{2}\mathrm{Li}_2\left(-\frac{(1-v)^2}{(1+v)^2}\right) - \frac{1}{2}\mathrm{Li}_2\left(-\frac{(1+v)^2}{(1-v)^2}\right),$$

$$t_{0+}^{ba}(w) = -2\ln\left(\frac{1+v}{1-v}\right)\ln(w_0+w) + \mathrm{Li}_2\left(\frac{w_0+w}{w_0+1}\right) - \mathrm{Li}_2\left(\frac{w_0+w}{w_0-1}\right) + \mathrm{Li}_2\left(\frac{a(w_0+w)}{aw_0+b}\right) - \mathrm{Li}_2\left(\frac{a(w_0+w)}{aw_0-b}\right),$$

$$t_{0-}^{z}(w) = \frac{1}{2}\ln\left(\frac{\xi}{1-\xi}\right)\ln(w_0-w) - \frac{1}{2}\ln^2(w_0-w) + \mathrm{Li}_2\left(\frac{w_0-w}{2w_0}\right) - \mathrm{Li}_2\left(\frac{w_0-w}{w_0-1}\right) - \mathrm{Li}_2\left(\frac{w_0-w}{w_0+1}\right),$$

$$t_{0+}^{z}(w) = -\frac{1}{2}\ln\left(\frac{\xi}{1-\xi}\right)\ln(w_0+w) + \frac{1}{2}\ln^2(w_0+w) - \mathrm{Li}_2\left(\frac{w_0+w}{2w_0}\right) + \mathrm{Li}_2\left(\frac{w_0+w}{w_0-1}\right) + \mathrm{Li}_2\left(\frac{w_0+w}{w_0+1}\right),$$

$$t_{0-}^{ab}(w) = -\ln\xi\ln(w_0-w) + \mathrm{Li}_2\left(\frac{a(w_0-w)}{aw_0-b}\right) + \mathrm{Li}_2\left(\frac{a(w_0-w)}{aw_0+b}\right) - \mathrm{Li}_2\left(\frac{w_0-w}{w_0-1}\right) - \mathrm{Li}_2\left(\frac{w_0-w}{w_0+1}\right),$$

$$t_{0+}^{ab}(w) = \ln\xi\ln(w_0+w) - \mathrm{Li}_2\left(\frac{a(w_0+w)}{aw_0-b}\right) - \mathrm{Li}_2\left(\frac{a(w_0+w)}{aw_0+b}\right) + \mathrm{Li}_2\left(\frac{w_0+w}{w_0-1}\right) + \mathrm{Li}_2\left(\frac{w_0+w}{w_0+1}\right),$$

$$t_{0-}^{\lambda}(w) = -\ln\left(\frac{2\lambda}{1-2\lambda+\sqrt{\xi}}\right)\ln(w_0-w) + \mathrm{Li}_2\left(\frac{w_0-w}{w_0-w_\lambda}\right) + \mathrm{Li}_2\left(\frac{w_0-w}{w_0+w_\lambda}\right) - \mathrm{Li}_2\left(\frac{w_0-w}{w_0-1}\right) - \mathrm{Li}_2\left(\frac{w_0-w}{w_0+1}\right),$$

$$t_{0+}^{\lambda}(w) = \ln^2(w_0+w) - \ln(1-w_0^2)\ln(w_0+w) + \mathrm{Li}_2\left(\frac{w_0-w_\lambda}{w_0+w}\right) + \mathrm{Li}_2\left(\frac{w_0+w_\lambda}{w_0+w}\right) + \mathrm{Li}_2\left(\frac{w_0+w}{w_0-1}\right) + \mathrm{Li}_2\left(\frac{w_0+w}{w_0+1}\right), \tag{C18}$$

$$t_{1-}^{ba}(w) = \ln^2(1-w) + \ln\left(\frac{a}{8}\right)\ln(1-w) + \mathrm{Li}_2\left(\frac{2\sqrt{\xi}}{a(1-w)}\right) + \mathrm{Li}_2\left(\frac{a(1-w)}{4}\right) + \mathrm{Li}_2\left(\frac{1-w}{2}\right),$$

$$t_{1+}^{ba}(w) = \ln^2(1+w) + \ln\left(\frac{a}{8}\right)\ln(1+w) + \mathrm{Li}_2\left(\frac{2\sqrt{\xi}}{a(1+w)}\right) + \mathrm{Li}_2\left(\frac{a(1+w)}{4}\right) + \mathrm{Li}_2\left(\frac{1+w}{2}\right),$$

$$t_{1-}^{z}(w) = -\ln\left(\frac{1+w_0}{2}\right)\ln(1-w) - \mathrm{Li}_2\left(\frac{1-w_0}{1-w}\right) + \mathrm{Li}_2\left(\frac{1-w}{1+w_0}\right) - \mathrm{Li}_2\left(\frac{1-w}{2}\right),$$

$$t_{1+}^{z}(w) = \ln\left(\frac{1+w_0}{2}\right)\ln(1+w) - \mathrm{Li}_2\left(\frac{1+w}{1-w_0}\right) + \mathrm{Li}_2\left(\frac{1+w_0}{1+w}\right) + \mathrm{Li}_2\left(\frac{1+w}{2}\right),$$

$$t_{1-}^{ab}(w) = -\ln(2a)\ln(1-w) - \mathrm{Li}_2\left(\frac{2\sqrt{\xi}}{a(1-w)}\right) + \mathrm{Li}_2\left(\frac{a(1-w)}{4}\right) - \mathrm{Li}_2\left(\frac{1-w}{2}\right),$$

$$t_{1+}^{ab}(w) = \ln(2a)\ln(1+w) + \mathrm{Li}_2\left(\frac{2\sqrt{\xi}}{a(1+w)}\right) - \mathrm{Li}_2\left(\frac{a(1+w)}{4}\right) + \mathrm{Li}_2\left(\frac{1+w}{2}\right),$$

$$t_{1-}^{\lambda}(w) = \frac{1}{2}\ln^2(1-w) + \ln 2\ln(1-w) - \ln(1-w_\lambda^2)\ln(1-w) + \mathrm{Li}_2\left(\frac{1-w}{1-w_\lambda}\right) + \mathrm{Li}_2\left(\frac{1-w}{1+w_\lambda}\right) - \mathrm{Li}_2\left(\frac{1-w}{2}\right),$$

$$t_{1+}^{\lambda}(w) = \frac{1}{2}\ln^2(1+w) - \ln 2\ln(1+w) + \mathrm{Li}_2\left(\frac{1-w_\lambda}{1+w}\right) + \mathrm{Li}_2\left(\frac{1+w_\lambda}{1+w}\right) + \mathrm{Li}_2\left(\frac{1+w}{2}\right). \tag{C19}$$

[1] G. Grunberg, Y. J. Ng, and S. H. H. Tye, Phys. Rev. D **21**, 62 (1980).
[2] J. Jersák, E. Laermann, and P. M. Zerwas, Phys. Rev. D **25**, 1218 (1982); **36**, 310(E) (1987).
[3] R. Jost and J. Luttinger, Helv. Phys. Acta **23**, 201 (1950); J. Schwinger, *Particles, Sources and Fields* (Addison-Wesley, New York, 1973), Vol. II, Sec. 5.4.
[4] J. B. Stav and H. A. Olsen, Z. Phys. C **57**, 519 (1993).
[5] J. B. Stav and H. A. Olsen, Phys. Rev. D **52**, 1359 (1995).
[6] M. M. Tung, J. Bernabéu, and J. Peñarrocha, Nucl. Phys. **B470**, 41 (1996).
[7] J. G. Körner, A. Pilaftsis, and M. M. Tung, Z. Phys. C **63**, 575 (1994).
[8] S. Groote, J. G. Körner, and M. M. Tung, Z. Phys. C **70**, 281 (1996).
[9] S. Groote and J. G. Körner, Z. Phys. C **72**, 255 (1996).
[10] S. Groote, J. G. Körner, and M. M. Tung, Z. Phys. C **74**, 615 (1997).

[11] V. Ravindran and W. L. van Neerven, Nucl. Phys. **B589**, 507 (2000).
[12] J. B. Stav and H. A. Olsen, Phys. Rev. D **54**, 817 (1996).
[13] A. B. Arbuzov, D. Y. Bardin, and A. Leike, Mod. Phys. Lett. A **7**, 2029 (1992); **9**, 1515(E) (1994).
[14] Y. Akatsu and O. Terazawa, Int. J. Mod. Phys. A **12**, 2613 (1997).
[15] M. Fischer, S. Groote, J. G. Körner, and M. C. Mauser, Phys. Rev. D **65**, 054036 (2002).
[16] J. Kodaira, T. Nasuno, and S. J. Parke, Phys. Rev. D **59**, 014023 (1998).
[17] W. Bernreuther, U. Löw, J. P. Ma, and O. Nachtmann, Z. Phys. C **43**, 117 (1989).
[18] J. G. Körner, J. P. Ma, R. Münch, O. Nachtmann, and R. Schöpf, Z. Phys. C **49**, 447 (1991).
[19] S. J. Parke and Y. Shadmi, Phys. Lett. B **387**, 199 (1996).
[20] A. Czarnecki, M. Jeżabek, J. G. Körner, and J. H. Kühn, Phys. Rev. Lett. **73**, 384 (1994).
[21] A. Czarnecki and M. Jeżabek, Nucl. Phys. **B427**, 3 (1994).
[22] J. G. Körner and D. Pirjol, Phys. Rev. D **60**, 014021 (1999).
[23] S. Groote, W. S. Huo, A. Kadeer, and J. G. Körner, Phys. Rev. D **76**, 014012 (2007).
[24] M. Fischer, S. Groote, J. G. Körner, M. C. Mauser, and B. Lampe, Phys. Lett. B **451**, 406 (1999).
[25] H. S. Do, S. Groote, J. G. Körner, and M. C. Mauser, Phys. Rev. D **67**, 091501(R) (2003).
[26] G. J. Gounaris, M. Kuroda, and F. M. Renard, Phys. Rev. D **54**, 6861 (1996).
[27] O. Antipin and G. Valencia, Phys. Rev. D **79**, 013013 (2009).